Topographic effect in a Faraday experiment

1999 J. Phys. A: Math. Gen. 32 6963

(http://iopscience.iop.org/0305-4470/32/40/306)

J. Phys. A: Math. Gen. **32** (1999) 6963–7000. Printed in the UK PII: S0305-4470(99)97912-X

Topographic effect in a Faraday experiment

Sh U Galiev

Department of Mechanical Engineering, The University of Auckland, Private Bag 92019, Auckland 1, New Zealand

Received 28 September 1998, in final form 22 April 1999

Abstract. Surface waves in water or granular layers and on the surface of weakly cohesive upper-lying soils are studied. A one-dimensional perturbed wave equation is derived for these waves. It is shown that the waves may be excited due to local topographies and a vertical excitation. The velocity of the waves depends on the geometry of the layer, the mechanical properties of the material and the vertical forced acceleration. Approximate solutions of the equation are presented which take into account resonant, nonlinear, dispersive, dissipative, topographic and parametric effects. The solutions describe *unfamiliar* waves which cannot be classified as soliton-, cnoidal-, shock- or breather-type waves. In particular, the solutions describe *spatiotemporally oscillating*, localized, nonlinear, surface waves which possess properties of both *standing* waves and *travelling* waves. They are not d'Alembert-type waves. Different wave patterns are yielded by the solutions in the x–t plane. Topographic and parametric effects are analysed. Sometimes these effects are dependent. The topographic effect explains some unexpected results of both experiments and earthquakes. An observation of Charles Darwin is discussed. Perhaps the solutions describe waves which may be in different wave fields of Nature.

1. Introduction and governing equation

Following Chladni's research, Faraday [1] explored vertically vibrated layers of sand-like materials and liquid. He found that small mounds formed. For liquid, surface waves oscillating at precisely half the forcing frequency of the bed were discovered. Rayleigh [2] suggested that the waves were the result of the parametric resonance. This idea was developed in different publications [3, 4]. Recent experimental studies of vertically vibrated liquid or granular media demonstrated a rich variety of nonlinear wave phenomena, depending on the amplitude and frequency of the excitation [5–8]. Physicists suggested these phenomena were possibly relevant to areas of physics as remote as semiconductors, earthquakes and clustering of galaxies. In particular, spatially localized, oscillating excitations (oscillons) were observed [6] on the surface of a layer of vertically vibrated brass balls. Recently, a few models [9] have been proposed, useful for interpretation of the experimental data. Results of numerical simulations were presented for layers having a constant thickness [9].

However, perturbations of the thickness of the layer may be important for the vertically excited surface waves. Oscillons did not form spontaneously from the flat layer. One can start these waves by touching the 'sand' surface with a pencil [7]. According to [8] the lateral motion of grains is possible if there is some slope of the free surface. Soliton-type travelling waves can be excited on the surface of the vertically vibrated heap of sand [5]. Thus, the vertically excited oscillations may be generated and amplified due to local topographies on the layer surface. Indeed, amplification of seismic waves due to topographies is a well known effect in seismology. Apparently, Charles Darwin [10] first highlighted crest amplification when

0305-4470/99/406963+38$30.00

he described the results of the 20 February 1835 Chilean earthquake. A local amplification, observed in the field, can reach a factor of 75 [11]. This agrees with analytical investigations of resonant seismic waves [12] which were published recently (see also [13]).

We shall consider in this paper waves which are long with respect to thickness h of the surface layer. The composition of the layers is considered as a compound of pure material (solid or liquid phase) and gas. Let us assume that the exchange of the mass, momentum and energy between the gas and the pure material is negligible. The gas and the pure material have the same velocity and pressure. Particles of the pure material are elastic and very small. Due to the above assumption we can describe the behaviour of the material by the equations of continuum where space-averaged values are used. Properties of the material, as a two-phase medium, will be described with the help of a state equation.

In what follows, one-dimensional equations are presented for surface waves in layers having a slightly varying thickness h. In this section, a perturbed wave equation is derived for weakly nonlinear waves. These equations are written with the help of unknown values which are averaged over the thickness. As an example of the averaging, we give an expression for the thickness-averaged pressure P: $P - P_a = h_0^{-1}\int_0^{h_0}(P_* - P_a)\,\mathrm{d}y$, where h_0 is a mean thickness of the layer, y is a vertical coordinate directed upwards from the bed, P_* is the pressure depending on y, and P_a is the atmospheric pressure. Let us assume for pressure P_* the following law: $P_* - P_a = \rho g(h - y + \eta)$, where ρ is the density, $g = g_0 + g_y$, g_0 is the acceleration due to gravity, $g_y = g_y(t)$ is the excited acceleration of the layer and η denotes an elevation of the surface. On the vibrating bed $y = 0$ and $P_* - P_a = \rho g(h + \eta)$. On the free surface $y = h + \eta$ and $P_* - P_a = 0$. The above law for the pressure is the basis of the theory of shallow-water waves.

Basic equations. Following Airy's method [14] and introducing averaged unknowns we can write equations of motion and continuity for the surface layer:

$$\rho_0 h(u_{tt} - X) = \sigma_x(h + \eta) \tag{1}$$

$$h = (h + \eta)(1 + u_x). \tag{2}$$

Here t is time, x is a horizontal Lagrangian coordinate, u is a horizontal displacement, X is a horizontal acceleration, σ is a stress, and subscripts t and x indicate the time and space derivatives, respectively. For the mean density ρ_0 we have $\rho_0 = \rho^0(1 - \phi_0) + \rho_{0g}\phi_0$, where ϕ_0 is the mean voidage (volume of the gas averaged over the thickness of the layer), ρ^0 and ρ_{0g} are the densities of the pure material and gas, respectively.

We assume a viscous model for the material. For upperlying thin layers and the weakly cohesive materials with the voidage fraction ϕ, this model is presented as

$$\sigma = -P + P_a + 4[\nu(1 - \alpha_s\phi)u_x + \eta^*(1 - \alpha_\nu\phi)u_{xt}]/3 \tag{3}$$

where ν and η^* are the elastic shear modulus and an effective viscosity, respectively. The latter is a function of the material viscosity and the bottom friction. We emphasize that η^* can depend on the time during the vertical excitation ($\eta^* = \eta^*(t)$). In particular, for the flying time the bottom friction disappears. An approximate dependence of η^* on the time will be presented in section 4.1. Coefficients α_s and α_ν in (3) are experimentally defined constants. They depend strongly on properties, an interaction and a quantity of the particles in a unit volume of the material. In (3) values $\alpha_s\phi$ and $\alpha_\nu\phi$ lie between 0 and 1. These values take into account the dependence of properties of the material and the layer on the voidage ϕ. If $\alpha_s\phi \to 1$, then the material transits into the so-called fluidized state and dissipative properties of the material can reduce according to (3).

We can write, following the theory of shallow waves [14, 15], the improved expression for the pressure:

$$P - P_+a = \rho h_0^{-1} \int_0^{h_0} \left[g(h - y + \eta) + \int_y^{h+\eta} \zeta_{tt}^* \, \mathrm{d}y \right] \mathrm{d}y \tag{4}$$

where ζ^* is a vertical displacement. Following Boussinesq [16] we shall assume that this displacement is the function of the elevation of the free surface:

$$\zeta^* = \eta(h + \eta)^{-m} y^m. \tag{5}$$

Here m is an integer and $m \geqslant 1$. The original work of Boussinesq [16] was restricted to an incompressible homogeneous inviscid fluid where $m = 1$. One can see that, according to formula (4), the pressure can have a large negative value if g has a large negative value and ρ is constant. However, this result is impossible for long waves and gassy, weakly cohesive media (water, granular materials and some soils). Therefore, we must take into account the compressibility of the materials. In particular, the gas extends in tension zones (the cavitation phenomenon) and changes completely the properties of the material. For the compound an equation of state may be presented in the following way:

$$\rho = \rho_0\{(1 - \phi_0)[1 - \lambda(P - P_a)] + \phi\}^{-1} \tag{6}$$

where λ is the compressibility of the pure material. Equation (6) was given in [17] and used in [18] where waves in a bubbly liquid were studied. A modified equation (6) was given in [12] for a particle–air–liquid mixture. We can now express the connection between the gas volume and the pressure. For the long waves the gas oscillations may be considered as isothermal. Therefore, we have the following connection:

$$P = P_a \rho_g \rho_{0g}^{-1} = P_a \phi_0 \phi^{-1}. \tag{7}$$

Taking into account (7) we rewrite equation (6) as $\lambda P^2 - [1 + \lambda P_a - \rho_0 \rho^{-1}(1 - \phi_0)^{-1}]P - P_a\phi_0(1 - \phi_0)^{-1} = 0$. The latter yields that

$$P = 0.5\lambda^{-1}(1 - \phi_0)^{-1}\{b_0 + [b_0^2 + 4\lambda\phi_0 P_a(1 - \phi_0)]^{0.5}\} \tag{8}$$

where $b_0 = (1-\phi_0)(1+\lambda P_a) - \rho_0\rho^{-1}$. According to (8) the pressure in the layer always exceeds zero if $\phi_0 \neq 0$. Generally speaking, we can use (8) as a state equation for the layer material. This equation shows that the pressure in the layer is positive for any vertical excitation, even when $\rho \to 0$.

Equations (1)–(7) form a strictly nonlinear system for the elevation of the surface and the thickness-average displacement, pressure, density and voidage. The vertical displacement is defined by (5) for different m. Thus the variation of the average and the non-average displacement, pressure, density and voidage, along the vertical coordinate y may be studied with the help of system (1)–(7). Let us consider weakly nonlinear surface waves. This case may be studied by the perturbation method.

Weakly nonlinear waves. It follows from equations (1) and (2) that $\rho_0(1+u_x)(u_{tt} - X) = \sigma_x$. Then one can obtain using (3) that

$$\begin{aligned}\rho_0(1 + u_x)(u_{tt} - X) = &-P_x + 4[\nu(1 - \alpha_s\phi)u_{xx} + \eta^*(1 - \alpha_\nu\phi)u_{xxt}]/3 \\ &-4\phi_x(\nu\alpha_s u_x + \eta^*\alpha_\nu u_{xt})/3.\end{aligned} \tag{9}$$

Let us express P_x in (9) with the help of u, assuming that $m = 1$ in (5). One can find from (4) that

$$\begin{aligned}p = P - P_0 = &-g_0\rho_0(h - 0.5h_0) + g\rho(h - 0.5h_0 + \eta) + 0.5\rho[(\eta + h)^2 - h_0^2/3] \\ &\times\{\eta_{tt}[(\eta + h)^{-1} - \eta(\eta + h)^{-2}] - 2\eta_t^2[(\eta + h)^{-2} - \eta(\eta + h)^{-3}]\}\end{aligned}$$

where $P_0 = P_a + g_0\rho_0(h - 0.5h_0)$. For simplicity we assume here that $h \gg \eta$ and $P_0 \gg g_0\rho_0(h - 0.5h_0)$. In this case, approximately, $p = g\rho(h - 0.5h_0 + \eta) + \rho h_0\eta_{tt}/3$ and, according to (6), $\rho = \rho_0(1 - \phi_0 + \phi)^{-1}$. We neglected in the latter the compressibility of the pure material. As a result one can write the next equation for p:

$$p(1 + \phi - \phi_0) = g\rho_0\eta + g\rho_0(h - 0.5h_0) + \rho_0 h_0\eta_{tt}/3. \tag{10}$$

Here, according to (2) and (7), we have $\eta = -hu_x(1 + u_x)^{-1} = -hu_x(1 - u_x + u_x^2 - \cdots)$, $\phi = \phi_0(1 + pP_0^{-1})^{-1} = \phi_0(1 - pP_0^{-1} + p^2P_0^{-2} - p^3P_0^{-3}\ldots)$. Now, by the iteration method, one can find from (10) the perturbation p as a function of the displacement u. The first approximation is $p = g\rho_0(h - 0.5h_0 - hu_x)$. The second approximation yields

$$p = b_2 - b_1u_x + b_3u_x^2 - g\rho_0h_0^3u_{xxx}/3$$

where

$$b_1 = gh\rho_0[1 + g\rho_0(2h - h_0)\phi_0P_0^{-1}]$$
$$b_2 = g\rho_0(h - 0.5h_0)[1 + g\rho_0(h - 0.5h_0)\phi_0P_0^{-1}]$$
$$b_3 = gh\rho_0(1 + gh\rho_0\phi_0P_0^{-1}).$$

One can see that the second approximation depends on the mean voidage. The third approximation we shall present as

$$p = P - P_0 = g\rho_0(h - 0.5h_0) - \phi_0g^2\rho_0^2(h - 0.5h_0)^2P_0^{-1} - gh\rho_0(1 - u_x + u_x^2)u_x$$
$$-\phi_0h_0^2g^2\rho_0^2P_0^{-1}u_x - g\rho_0h_0^3u_{xxx}/3. \tag{11}$$

We assumed for the thin layers that $\phi_0 \ll 1$, $|h/h_0 - 1| \ll 1$ and neglected in (11) small terms containing $\phi_0^2h_0^2$ or $\phi_0h_0^3$. Now expression (11) is substituted in (9). Let the dissipative term in (9) be second order with respect to u. Nonlinear terms will be considered in (9) which do not depend explicitly on the dissipative and dispersive effects. It is also assumed that linear and nonlinear terms containing partial derivatives of h (for example, ρgh_xu_x) are negligible. This simplifies the analysis of the influence of nonlinearity, topography and the parametric effect on the surface waves. Taking into account the comments above, one can obtain from (9) and (11) the following equation:

$$\rho_0(u_{tt} - X) - [gh\rho_0 + \phi_0g^2h_0^2\rho_0^2P_0^{-1} + \tfrac{4}{3}\nu(1 - \phi_0\alpha_s)]u_{xx} = -g\rho_0h_x + \tfrac{4}{3}\eta^*(1 - \phi_0\alpha_\nu)u_{xxt}$$
$$+g\rho_0h_0^3u_{xxxx}/3 - [3gh\rho_0 + \tfrac{4}{3}\nu(1 - \phi_0\alpha_s)]u_xu_{xx}$$
$$+[6gh\rho_0 + \tfrac{4}{3}\nu(1 - \phi_0\alpha_s)]u_x^2u_{xx}. \tag{12}$$

Some coefficients in (12) depend on ϕ_0. Generally speaking, the voidage ϕ_0 depends on the amplitude and the frequency of the forced oscillations. If the variation of ϕ_0 is very small then we can neglect this dependence over a few oscillations and use equation (12). However, this effect can accumulate and change the coefficients in (12) over a long period of time. According to [19] this process may be studied with the help of the fully nonlinear equations (1)–(7). Below we shall consider a case when ϕ_0 is constant. It is also assumed that $|gh\rho_0| \gg \phi_0g^2h_0^2\rho_0^2P_0^{-1}$. For this case equation (12) may be rewritten so that

$$u_{tt} - a_0^2u_{xx} = -gh_x + \beta u_xu_{xx} + \beta_1u_{xx}u_x^2 + \mu u_{txx} + ku_{xxxx} - X \tag{13}$$

where $a_0^2 = a_f^2 + a_s^2$, $a_f^2 = gh$, $a_s^2 = \frac{4}{3}\nu\rho_0^{-1}(1 - \phi_0\alpha_s)$, $\beta = -3a_f^2 - a_s^2$, $\beta_1 = 6a_f^2 + a_s^2$, $\mu = \frac{4}{3}\eta^*(1 - \phi_0\alpha_\nu)\rho_0^{-1}$ and $k = gh_0^3/3$. The term $a_0^2u_{xx}$ takes into account the parametric effect, since $a_0^2 = gh + a_s^2$ and g is a time-dependent acceleration. The nonlinear terms in (13) are of second and third order with respect to u. The dissipative term depends on the mean voidage. Generally speaking, the dissipative term is first order but we shall assume that this term and ku_{xxxx} are second order. The term gh_x in (13) takes into account the topographic

effect. Thus equation (13) combines both the topographic and parametric effects. We shall consider below a case when $X = 0$. Let $a_s^2 = 0$. In this case the velocity of the surface waves can have an imaginary value if $g = g_0 + g_y < 0$ and $\phi_0 = 0$. One can see from (12) that any voidage hinders the generation of the imaginary velocity and the imaginary velocity is impossible if ϕ_0 is large enough.

The wave velocity a_0 depends on the vertical acceleration and the thickness of the layer. For weakly cohesive media and an extensive vertical excitation this velocity may be strictly different during flying and contact times. Any voidage reduces a_0. On the other hand, the wave velocity is defined by the elastic shear modulus. One can see that the effects of the vertical acceleration and the thickness on the wave velocity is not important for tight materials. However, these effects may be important for weakly cohesive soils, liquefiable soils and soft media.

The amplitude of the earthquake-induced vertical acceleration may be of the order of 10 m s^{-2}. Let h be of order 10 m. In this case the parametric earthquake-induced long waves may be excited on the surface of noncohesive (or weakly cohesive) soils and the soft sediment according to the presented theory. In particular, the parametric earthquake-induced surface long waves may be excited in sea/soft sediment systems. At the same time these waves are impossible for the tight geomaterials according to (13).

Thus, the parametric effect depends on the level of the excitation and may be quite different for liquid and solid media [13]. At the same time, the topographic effect may be important for any excitation and both for solid and liquid media. We shall consider here the topographic effect for weak and extensive vertical excitations. For the former the parametric effect is not important. This case will be studied in sections 2 and 3. For extensive excitation both parametric and topographic effects may be important. This case will be considered in section 4.

Remark. Generally speaking, equation (13) describes the surface waves in any solid upperlying layers with a slightly variable thickness if model (3) and expression (4) for the pressure are valid. Equation (13) also describes a propagation of one-dimensional body waves in different media (bubbly liquid, porous rock, porous material saturated by a bubbly liquid and so on [12]) if $h_x = 0$. The coefficients in (13) for these media are presented in [12]. In particular, equation (13) was used for the study of resonant waves excited in different resonators [12, 13].

2. Forced and free waves (fixed boundaries)

2.1. Perturbation method

Nonlinear periodical waves in physical systems without dissipation and dispersion have been intensively studied [20]. Here, the waves in a closed driven-disspative–dispersive system will be explored when $g_y(t) \ll g_0$ and a_0 may be considered as constant. In this case the bottom friction depends weakly on time and, approximately, η^* is constant. As a result we have constant coefficients in (13). The latter may be solved by the method suggested in [21]. Let us introduce deformable coordinates r and s:

$$r = t - xa_0^{-1} + \beta u a_0^{-3}/4 \qquad s = t + xa_0^{-1} - \beta u a_0^{-3}/4. \tag{14}$$

Now one can find new expressions for terms in (13). For example, $u_t = u_r r_t + u_s s_t = u_r(1 + \beta u_t/4a_0^3) + u_s(1 - \beta u_t/4a_0^3) \approx (u_r + u_s)[1 + A_*(u_r - u_s) + A_*^2(u_r - u_s)^2]$, where the subscripts r and s refer to partial derivatives with respect to r and s. Then, neglecting terms of fourth order, we can rewrite (13) so that

$$u_{rs} = -ga_0^{-1}(h_s - h_r)/4 + A_*(u_s u_{ss} - u_r u_{rr}) + 0.25a_0^{-2}[\mu(u_{rrr} - u_{rrs} - u_{ssr} + u_{sss})$$

$$+k(u_{rrrr} - 2u_{rrss} + u_{ssss})] + a_* u_r u_s (u_{rr} + u_{ss}) + b_*[u_{rr}(u_s)^2 + u_{ss}(u_r)^2]$$
$$+c_*[u_{rr}(u_r)^2 + u_{ss}(u_s)^2]. \tag{15}$$

Here $A_* = \beta a_0^{-3}/4$, $a_* = 5A_*^2 - 2D_*$, $b_* = -2A_*^2 + D_*$, $c_* = -4A_*^2 + D_*$, $D_* = \beta_1/4a_0^4$. We did not take into account the influence of dispersion and dissipation on the nonlinear terms in (15). A solution of (15) is sought as a sum: $u = u_1 + u_2 + u_3$, where $u_1 \gg u_2 \gg u_3$. Thus a solution of (15) is sought by the perturbation method. This method has a broad application in physics. At the same time there is a serious difficulty with the application of this method. This difficulty has the form of the so-called 'secular terms' which are generated by nonlinearity and grow infinitely when $t \to \infty$. We shall meet these terms later. Substituting the sum into (15) and equating terms of the same order one can obtain the following linear differential equations:

$$u_{1rs} = -0.25 g a_0^{-1}(h_s - h_r) \tag{16}$$

$$u_{2rs} = A_*(u_{1s}u_{1ss} - u_{1r}u_{1rr}) + 0.25a_0^{-2}[\mu(u_{1rrr} - u_{1rrs} - u_{1ssr} + u_{1sss})$$
$$+k(u_{1rrrr} - 2u_{1rrss} + u_{1ssss})] \tag{17}$$

$$u_{3rs} = A_*(u_{1s}u_{2ss} + u_{2s}u_{1ss} - u_{1r}u_{2rr} - u_{2r}u_{1rr}) + a_* u_{1r}u_{1s}(u_{1rr} + u_{1ss})$$
$$+b_*[u_{1rr}(u_{1s})^2 + u_{1ss}(u_{1r})^2] + c_*[u_{1rr}(u_{1r})^2 + u_{1ss}(u_{1s})]^2. \tag{18}$$

The d'Alembert-type solution of the nonhomogeneous wave equation (16) is

$$u_1 = J_1(r) + j_1(s) - 0.25a_0^{-1}\iint g(h_s - h_r)\,\mathrm{d}r\,\mathrm{d}s. \tag{19}$$

Further, the wave-type solution of (17) is given by

$$u_2 = J_2^*(r) + j_2^*(s) - 0.5A_*\{s[J_1'(r)]^2 - r[j_1'(s)]^2\} + a_0^{-2}\{\mu[sJ_1''(r) + rj_1''(s)]$$
$$+k[sJ_1'''(r) + rj_1'''(s)]\}/4. \tag{20}$$

Here, the prime denotes differentiation with respect to the appropriate variable: r or s (14). Only bounded solutions of equation (13) are considered in this paper. The secular terms in (20) are eliminated if

$$J_2^*(r) = J_2(r) + 0.5rA_*[J_1'(r)]^2 - a_0^{-2}[\mu r J_1''(r) + kr J_1'''(r)]/4$$
$$j_2^*(s) = j_2(s) - 0.5sA_*[j_1'(s)]^2 - a_0^{-2}[\mu s j_1''(s) + ksj_1'''(s)]/4.$$

Using the expressions for u_1 and u_2 one can find u_3 from (18):

$$u_3 = J_3^*(r) + j_3^*(s) - A_* s J_1' J_2' + A_* r j_1' j_2' + a_*[j_1(J_1')^2 + J_1(j_1')^2]/2 + (b_* - A_*^2/2)$$
$$\times\left[J_1'\int (j_1')^2\,\mathrm{d}s + j_1'\int (J_1')^2\,\mathrm{d}r\right] + (c_*/3 - A_*^2/2)[r(j_1')^3 + s(J_1')^3]$$
$$+A_*^2(s^2/2 - rs)J_1''(J_1')^2 + A_*^2(r^2/2 - rs)j_1''(j_1')^2.$$

Here $J_1 = J_1(r)$, $j_1 = j_1(s)$, $J_2 = J_2(r)$, $j_2 = j_2(s)$. The secular terms are eliminated if

$$J_3^*(r) = J_3(r) + A_* r J_1' J_2' - (c_*/3 - A_*^2/2)r(J_1')^3 + A_*^2 r^2 J_1''(J_1')^2/2$$
$$j_3^*(s) = j_3(s) - A_* s j_1' j_2' - (c_*/3 - A_*^2/2)s(j_1')^3 + A_*^2 s^2 j_1''(j_1')^2/2.$$

Finally, the approximate bounded solution of (13), presented with the help of deformable coordinate r and s (14), is

$$u = J_1 + j_1 - 0.25a_0^{-1}\iint g(h_s - h_r)\,\mathrm{d}r\,\mathrm{d}s + J_2 + j_2 + 0.5A_*(r - s)[(J_1')^2 + (j_1')^2]$$
$$+a_0^{-2}(s - r)[\mu(J_1'' - j_1'') + k(J_1''' - j_1''')]/4 + A_*(r - s)(J_1'J_2' + j_1'j_2')$$
$$+J_3(r) + j_3(s) + 0.5a_*[j_1(J_1')^2 + J_1(j_1')^2] + (b_* - 0.5A_*^2)$$
$$\times\left[J_1'\int (j_1')^2\,\mathrm{d}s + j_1'\int (J_1')^2\,\mathrm{d}r\right] + (c_* - 1.5A_*^2)(r - s)[(j_1')^3 - (J_1')^3]$$
$$+0.5A_*^2(r - s)^2[J_1''(J_1')^2 + j_1''(j_1')^2] + xd + d_1. \tag{21}$$

Here J_1, j_1, J_2, j_2, $J_3(r)$, $j_3(s)$ are unknown functions defined by boundary conditions; d and d_1 are constants which take into account an initial state of the layer. The double integral in (21) takes into account the topographic effect. One can consider (21) as the approximate d'Alembert-type solution of the perturbed wave equation (13). If perturbations of the thickness of the layer due to the topography are small and $|h/h_0 - 1| \ll 1$, then the above theory is applicable. Various site topographies may be on the free surface and the underlying bed of the layer. They may be described by the standard Fourier expansion.

2.2. Boundary problem and basic equation

Let us assume that $h_x = \sum_i H_i \cos i\pi x/L (i = 0, 1, 2, 3, \ldots I)$ and $g_y = \delta \cos \omega t$ ($\delta \ll g_0$). A layer of variable thickness embedded in a rigid basin will be considered. The length of the layer is L. Lateral flanks of the basin are perpendicular to the bed. They are located at $x = 0$ and $x = L$. Thus, boundary conditions are

$$u = 0 \qquad \text{at} \quad x = 0 \qquad \text{and} \qquad x = L. \tag{22}$$

Linear oscillations. Following [13] one can find that $J_1(r) = F(r) - \varphi \cos \omega r + d_*$,

$$\begin{aligned} &j_1(s) = -F(s) - \varphi \cos \omega s + d_* \qquad \text{where} \quad \varphi = -0.5\delta \sum_i H_i[\omega^2 - (\pi i a_0/L)^2]^{-1} \\ &d_* = 0.5 g_0 L^2 \pi^{-2} a_0^{-2} \sum_i H_i i^{-2} \qquad \text{and} \\ &F(r) = \frac{\delta \sin \omega r}{2 \sin \omega L a_0^{-1} + k L \omega^3 a_0^{-3} \cos \omega L a_0^{-1}} \sum_i \frac{H_i[(-1)^i - \cos \omega L a_0^{-1}]}{[\omega^2 - (\pi i a_0/L)^2]} \\ &\qquad -0.5 d_2 a_0 L^{-1} r. \end{aligned} \tag{23}$$

Here $d_2 = g_0 L^2 \pi^{-2} a_0^{-2} \sum_i [(-1)^i - 1] H_i i^{-2}$. Thus, travelling horizontal waves are excited due to the vertical excitation if $h_x \neq 0$. The resonant frequencies of the layer are defined approximately as $\Omega_{lN} = \Omega_{Nl} + \omega^*$, where $\Omega_{Nl} = N\pi a_0/L$ and $\omega^* = k a_0 L^{-3} \pi^3 N^3 (-1)^{N+1}/2 (N = 1, 2, 3, \ldots)$. If the coefficient k is very small, we obtain $\Omega_{lN} = \Omega_{Nl}$. Thus, the dispersion shifts the resonant frequencies. For the case $\omega^2 = (\pi i a_0/L)^2$ in (23) the double integral in (21) must be recalculated. We shall concern ourselves with this topographic resonance in sections 4.4 and 4.5.

Nonlinear oscillations. Let us consider nonlinear oscillations excited near and at the resonant frequencies. In this case we suggest, considering the second boundary condition (22), that

$$|F(r)| \gg \varphi \cos \omega r - d_* \qquad |F(s)| \gg \varphi \cos \omega s - d_*. \tag{24}$$

Function $F(s)$ is expanded in Taylor's series at $x = L$:

$$\begin{aligned} F(s) &= F[r + 2N\pi/\omega + 2\omega^{-1} a_0^{-1} L(\omega_1 + \omega^*) - \beta a_0^{-3} u/2] \\ &= F(r) + 2\omega^{-1} a_0^{-1} L(\omega_1 + \omega^*) F'(r) + 2\omega^{-2} a_0^{-2} L^2 (\omega_1 + \omega^*)^2 F''(r) \\ &\quad + 4\omega^{-3} a_0^{-3} L^3 (\omega_1 + \omega^*)^3 F'''(r)/3 + \cdots \end{aligned} \tag{25}$$

where $\omega = \Omega_{lN} + \omega_1$ and ω_1 is a perturbation of a resonant frequency. It was assumed that $F(r + 2N\pi/\omega) = F(r)$ and $u = 0$ in (25). Then we rewrite the second boundary condition (22) using (21), (24) and expansion (25):

$$\begin{aligned} &-2N\pi(\omega_1 + \omega^*)\omega^{-2} F' - \tfrac{1}{2}\beta L a_0^{-4} (F')^2 + \mu^* L a_0^{-3} F'' + k^* L a_0^{-3} F''' \\ &\qquad = l \cos \omega t + Ld + d_1 + d_2 \end{aligned} \tag{26}$$

where $\mu^* = \mu - 2a_0\omega^{-2}L(\omega^* + \omega_1)^2$, $k^* = k - 4\omega^{-3}L^2(\omega^* + \omega_1)^3/3$, $l = \delta\sum_i H_i[\omega^2 - (\pi i a_0/L)^2]^{-1}[\cos\omega L a_0^{-1} - (-1)^i]$, and only the linear and quadratic terms are written. It should be emphasized that the dissipative and dispersive terms in (26) depend on ω. Equation (26) may be rewritten so that

$$(F' - 2R\pi^{-1}\sqrt{\varepsilon})^2 - \mu^*\omega a_0\beta^{-1}F'' - 0.5k^*a_0\omega^2\beta^{-1}F''' = \varepsilon\cos^2\tau. \tag{27}$$

Here $F' = \mathrm{d}F/\mathrm{d}\tau$. We introduced a modified time variable $\tau = \omega t/2$ and assumed that $\varepsilon = -4la_0^4(\beta L)^{-1}$, $R = -\pi a_0^3(\omega_1 + \omega^*)/(\beta\omega\varepsilon^{0.5})$ and $Ld + d_1 + d_2 = l + 2L\beta^{-1}\omega^{-2}a_0^2(\omega^* + \omega_1)^2$. Equation (27) is obtained in [13]. This is the perturbed compound Burgers–Korteweg–de Vries equation for the travelling wave. Generally speaking, this equation is valid for both vertical- and horizontal-excited waves [13]. Equation (27) has the nonlinear term that tends to produce a 'discontinuity' in the wave. The second term dissipates the wave through a viscous-like effect. The third term disperses the wave. Because of this term a solitary-like wave may be excited. One can see that a balance between these terms varies together with the excited frequency [13]. In particular, equation (27) may simplify to the perturbed Korteweg–de Vries or Burgers equations in the trans-resonant range. We will seek solutions of (27) in the form:

$$F' = \sqrt{\varepsilon}[2R/\pi + \Phi(\tau)\cos\tau] \tag{28}$$

where $\Phi(\tau)$ is an unknown function and R is a trans-resonant parameter. As a result we obtain the next basic equation:

$$a_1(\Phi' - \Phi\tan\tau) + a_2(\Phi'' - 2\Phi'\tan\tau - \Phi) = -\sqrt{\varepsilon}(1 - \Phi^2)\cos\tau. \tag{29}$$

Here $a_1 = \omega a_0\beta^{-1}(\mu - 2\varepsilon\beta^2\pi^{-2}a_0^{-5}LR^2)$, $a_2 = a_0\omega^2\beta^{-1}(3k + 4\beta^3\varepsilon^{3/2}\pi^{-3}a_0^{-9}L^2R^3)/6$.

2.3. Trans-resonant evolution of localized forced surface waves

Solutions for different particular cases of equation (29) are presented in [13]. Here a special case of equation (29) is considered when

$$|\Phi'| \gg \Phi\tan\tau \qquad \text{and} \qquad |\Phi''| \gg 2\Phi'\tan\tau + \Phi. \tag{30}$$

Thus, we will seek fast varying solutions. In this case equation (29) yields

$$a_1\Phi' + a_2\Phi'' = -\sqrt{\varepsilon}(1 - \Phi^2)\cos\tau. \tag{31}$$

Let the approximate solution of (31) be a sum of travelling waves:

$$\Phi(2\omega^{-1}\xi) = A\tanh(e\sin M^{-1}\xi - eR) + [B\sec h^2(e\sin M^{-1}\xi - eR) + C]\cos\xi \tag{32}$$

where A, B, C and e are unknown constants, $\xi = \frac{1}{2}[\omega t \pm (\omega a_0^{-1}x - \pi N) \mp A_*\omega u]$, and M will be defined later. It is assumed that $|e| \gg 1$, $\sin M^{-1}\xi - R \ll 1$ and $\sin\xi \ll 1$. For the last case the conditions (30) take place. Solution (32) describes the interaction and the competition between the nonlinear, viscous-like and dispersive-like effects. We will consider two scenarios of the competition in the trans-resonant range.

First scenario ($C \neq -B$). Expression (32), where $x = L$, is substituted into (31). Next, equating to zero nonlocalized terms, and terms contain $\sec h^2(e\sin M^{-1}\tau - eR)$, or $\sec h^4(e\sin M^{-1}\tau - eR)$ or $\tanh(e\sin M^{-1}\tau - eR)\sec h^2(e\sin M^{-1}\tau - eR)$ we obtain four equations:

$$a_2C\cos\tau = \varepsilon^{0.5}(1 - A^2 - C^2\cos^2\tau)\cos\tau \tag{33}$$

$$a_1M^{-1}eA\cos M^{-1}\tau + a_2B(4M^{-2}e^2\cos^2 M^{-1}\tau - 1)\cos\tau = -\varepsilon^{0.5}(A^2 - 2BC\cos^2\tau)\cos\tau \tag{34}$$

$$6a_2M^{-2}e^2\cos^2 M^{-1}\tau\cos\tau = -\varepsilon^{0.5}B\cos^3\tau \tag{35}$$

$$a_1M^{-1}eB\cos M^{-1}\tau\cos\tau + a_2M^{-2}e^2A\cos^2 M^{-1}\tau = -\varepsilon^{0.5}A(B + C)\cos^2\tau. \tag{36}$$

We used in (31) that

$$\sin M^{-1}\tau - R \ll 1 \qquad \sin\tau \ll 1 \qquad 2AC\varepsilon^{0.5}\tanh^3(e\sin M^{-1}\tau - eR)\cos^2\tau \approx 0$$
$$\sec h^2(e\sin M^{-1}\tau - eR)\sin M^{-1}\tau \approx 0 \tag{37}$$
$$\tanh(e\sin M^{-1}\tau - eR)\sec h^2(e\sin M^{-1}\tau - eR)\sin M^{-1}\tau \approx 0.$$

Thus solution (32) is practically correct if $\sin M^{-1}\tau - R \ll 1$, $\sin\tau \ll 1$ and $R \ll 1$. We suggest in (33)–(36) that

$$\cos M^{-1}\tau \approx \cos\tau. \tag{38}$$

Thus we consider the solution localized near points $\tau = M\pi K$ ($K = 1, 2, 3, \ldots$). One can see that only odd subharmonic ($M = 3, 5, 7, \ldots$) oscillations are described by (32), if (38) holds. These oscillations satisfy condition (25) for any odd resonant frequency and may be excited in odd trans-resonant frequency bands. We note that the subharmonic oscillations with $M = 3$ were observed in [22] near $\omega L a_0^{-1} = 3\pi$ ($N = 3$).

Due to (38) we obtain four algebraic equations from (33)–(36) for A, B, C and e. Generally speaking, these equations may be solved by numerical methods. However, we will consider here a few cases of an approximate solution of (33)–(36). The cases allow us to understand the evolution of the waves.

(I). $R^3 \approx -\frac{3}{4}k\pi^3 a_0^9\beta^{-3}\varepsilon^{-1.5}L^{-2}$. In this case $a_2 \approx 0$ and we have $B \approx 0$ from (35).

Then, (36), (33) and (34) yield $C \approx 0$, $A \approx \pm 1$ and $e \approx -\varepsilon^{0.5}a_1^{-1}AM$. The second approximation is

$$A \approx \pm(1 - 0.75C^2)^{0.5} \qquad B \approx -3C$$
$$e \approx -\varepsilon^{0.5}a_1^{-1}AM(1 + 5.25C^2) \tag{39}$$
$$C \approx 2a_2a_1^{-2}\varepsilon^{0.5}.$$

Thus, solution (32) defines the shock-type wave if $|e| \gg 1$. However, a soliton-type wave generates within the shock structure if $a_2 \neq 0$. According to (39) the amplitude of the soliton increases together with $|a_2|$.

(II). We assume that $|A| \approx |B|$. This is the case when the influence of the dissipation (the first term in (31)) and the dispersion (the second term in (31)) is approximately the same. Since $e^2 \gg |e|$ we have from (33)–(35) that

$$A \approx \pm 1 \qquad B \approx \pm 1 \qquad e \approx \pm M(-a_2^{-1}\varepsilon^{0.5}B/6)^{0.5} \qquad C \approx -B/6. \tag{40}$$

In this case solution (32) defines a wave which is too difficult to classify as a soliton- or shock-type wave. The sign in front of B is defined so that e is real.

(III). $R^2 \approx 0.5\mu\pi^2\varepsilon^{-1}\beta^{-2}a_0^5L^{-1}$. In this case $a_1 \approx 0$ and equation (31) must have the soliton-type solution. Therefore $A \approx 0$ and (33)–(35) and (38) yield

$$C \approx \pm 1 \qquad B \approx -3C \qquad e \approx \pm M(-0.5a_2^{-1}\varepsilon^{0.5}C)^{0.5}. \tag{41}$$

The sign in front of C is defined so that e is real. Now we can correct A using (36) so that

$$A \approx -3a_1a_2^{-1}e^{-1}M. \tag{42}$$

Thus, within the soliton-type wave the shock-type wave is generated.

Generally speaking, solution (32) may be also valid behind the wave front if $AC\tanh^3(e\sin M^{-1}\tau) \ll 1$. The last restriction is not very severe because AC may be very small in (37) (see (39), (40) and (42)).

Second scenario ($C = -B$). If $C = -B$ then we have from (32)

$$\Phi(2\omega^{-1}\xi) = A\tanh(e\sin M^{-1}\xi - eR) - B\tanh^2(e\sin M^{-1}\xi - eR)\cos\xi. \tag{43}$$

Expression (43), where $x = L$, is substituted into (31). Next, equating to zero the nonlocalized terms and terms containing $\sec h^2(e\sin M^{-1}\tan -eR)$ or $\tanh(e\sin M^{-1}\tau - eR)\sec h^2(e\sin M^{-1}\tau - eR)$, we obtain three equations:

$$a_2 B\cos\tau = \varepsilon^{0.5}(A^2 - 1 + B^2\cos^2\tau)\cos\tau \tag{44}$$

$$a_1 M^{-1} eA\cos M^{-1}\tau - a_2 B(2M^{-2}e^2\cos^2\cos^2 M^{-1}\tau + 1)\cos\tau$$
$$= -\varepsilon^{0.5}(A^2 + B^2\cos^2\tau)\cos\tau \tag{45}$$

$$a_1 M^{-1} eB\cos M^{-1}\tau\cos\tau + a_2 M^{-2}e^2 A\cos^2 M^{-1}\tau = 0. \tag{46}$$

Considering (31) and solution (43) we assume

$$\begin{aligned} &2\varepsilon^{0.5}AB\tanh^3(e\sin M^{-1}\tau - eR) \approx 0\\ &6a_2 e^2 M^{-2}B\sec h^2(e\sin M^{-1}\tau - eR)\tanh^2(e\sin M^{-1}\tau - eR) \approx 0\\ &\sec h^2(e\sin M^{-1}\tau - eR)\sin M^{-1}\tau \approx 0\\ &\varepsilon^{0.5}B^2\sec h^2(e\sin M^{-1}\tau - eR)\tanh^2(e\sin M^{-1}\tau - eR) \approx 0. \end{aligned} \tag{47}$$

Due to (38) we obtain three algebraic equations from (44)–(46) for A, B and e. The following cases are now considered.

(IV). $R^3 \approx -\frac{3}{4}k\pi^3 a_0^9\beta^{-3}\varepsilon^{-.15}L^{-2}$. In this case $a_2 \approx 0$ and equation (46) yields that $B \approx 0$. As the first approximation we have from (44) and (45, respectively: $A \approx \pm 1$, $e \approx \varepsilon^{0/.5}a_1^{-1}AM$. Then we correct B using (46). As a result, $B \approx a_2 a_1^{-2}\varepsilon^{0.5}$. Thus, a soliton-type wave generates within the shock structure. This case is reminiscent of case (I).

(V). $|A| \approx |B|$. Equations (44) and (45) yield $A \approx \pm\sqrt{4/7}$, $B \approx \pm\sqrt{4/7}$, $e \approx \pm M(\varepsilon^{0.5}a_2^{-1}B)^{0.5}$. The sign in front of B is defined so that e is real.

(VI). $R^2 \approx 0.5\mu\pi^2\varepsilon^{-1}\beta^{-2}a_0^5 L^{-1}$. In this case $a_1 \approx 0$ and, evidently, $A \approx 0$. Then $B \approx \pm 1$ and one can find from (45) that $e \approx \pm M(-0.5a_2^{-1}\varepsilon^{0.5}B)^{0.5}$. The sign in front of B is defined so that e is real. Now it is possible to correct A. Using (46) one can find that $A \approx a_1 a_2^{-1}e^{-1}M$.

Solution (43) is valid if (47) takes place. Strictly speaking, this solution describes waves only near points where $\sin M^{-1}\tau - R \ll 1$ and $\sin\tau \ll 1$.

In figures 1 and 2 the surface waves calculated according to (32) and (28) are presented. Dimensionless coordinate (x/L) and the linear expression for elevation η were used. For simplicity we put $R = 0$. The amplitude of the waves changes, and they can form different patterns in the trans-resonant range. We note that figure 1(c) corresponds to figure 1 from [8] (see also section 4.5). From solution (43) pictures follow which are reminiscent of figures 1 and 2.

Thus in the trans-resonant bands *unfamiliar* waves are generated. The amplitude and the form of these waves depend strictly on the excited frequency. A front of the waves may be localized. Behind the localization the high-frequency waves may be generated in some media [22, 23]. For this case the solutions (32) and (43) must be corrected.

2.4. General solutions for forced waves in a rigid basin

Behind the fast-varying front $\Phi'' \approx \Phi$ and equation (29) may be rewritten so that

$$\Phi'' - \Phi = q_0^{-1}(1 - \Phi^2) \tag{48}$$

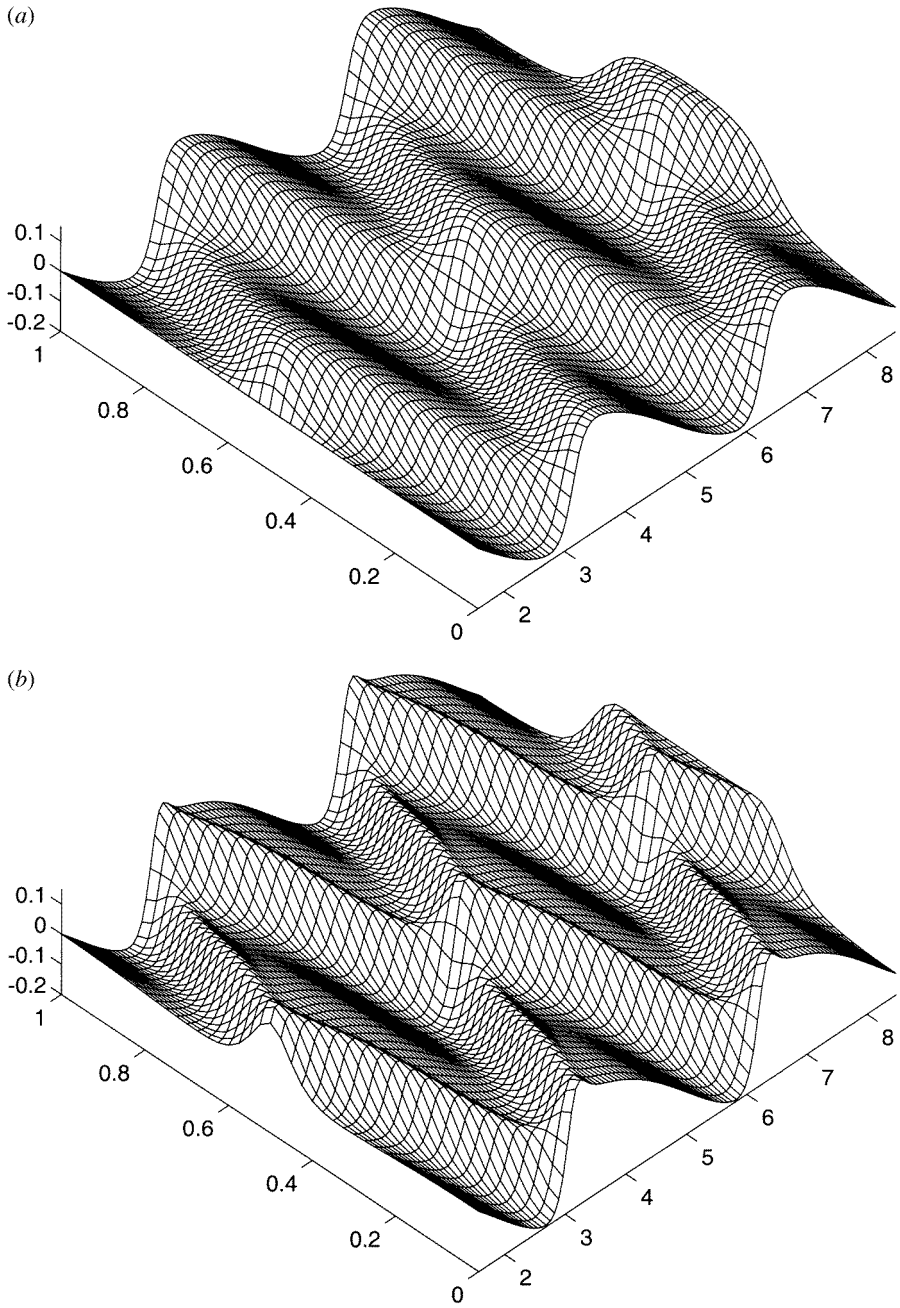

Figure 1. Waves excited near the fundamental resonance ($N = 1, M = 1$). (*a*) Case (I) and $A = 1$. (*b*) Case (II). (*c*) Case (III). (*d*) Case (I) and $A = -1$.

where $q_0 = -k^* a_0 \omega^2/(2\beta\sqrt{\varepsilon})$. We assumed that the dissipative effect localizes in the front. It is known that the Korteweg–de Vries equation (48) has a cnoidal-wave-type solution. Generally speaking, this solution is expressed by Jacobi elliptic functions. However, the topic of this paper is the approximate consideration of the wave processes. We will seek an approximate

(*c*)

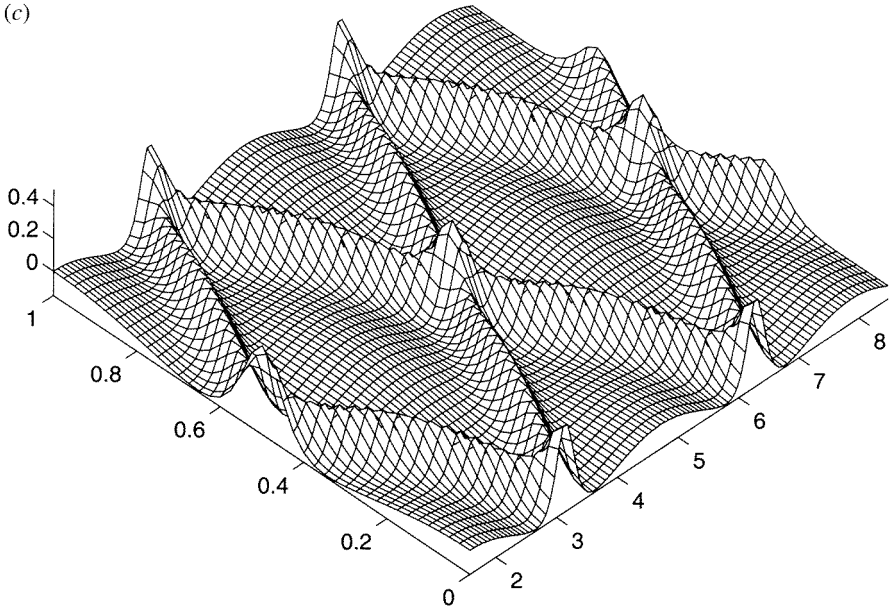

(*d*)

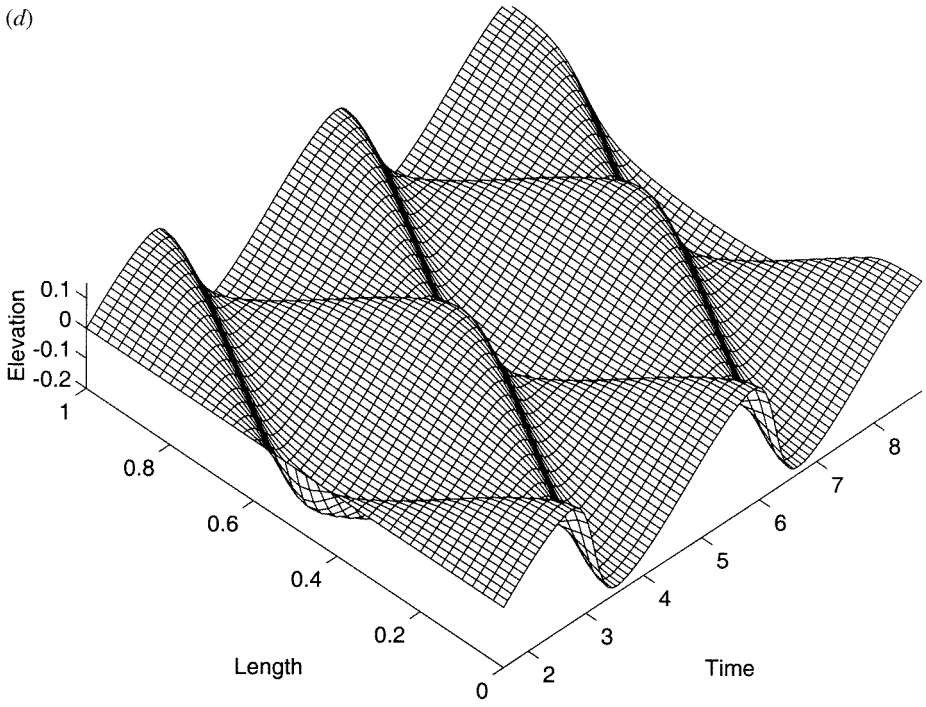

Figure 1. (Continued)

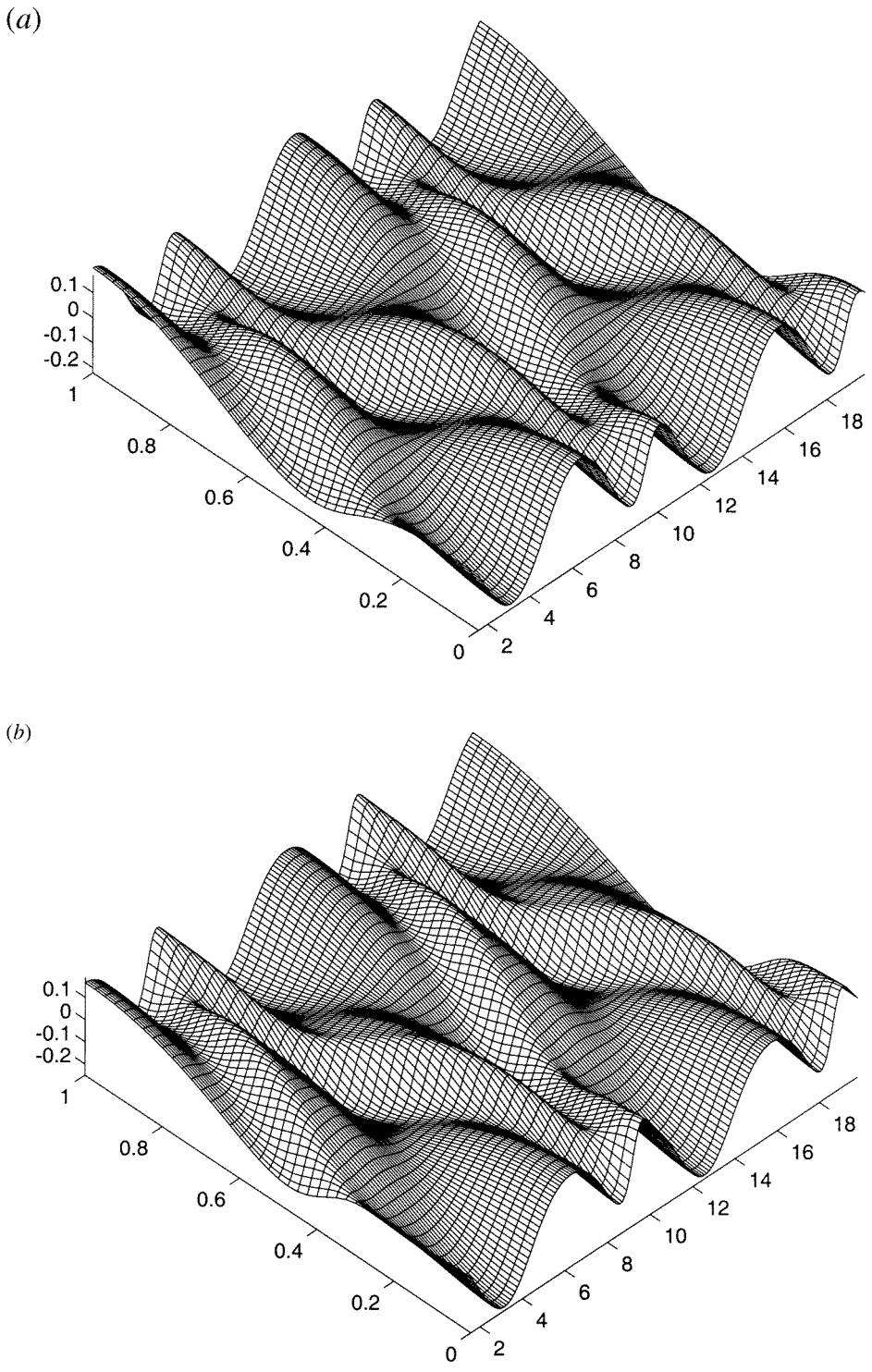

Figure 2. Subharmonic resonant waves ($N = 3$, $M = 3$). (*a*) Case (I) and $A = 1$. (*b*) Case (II). (*c*) Case (III). (*d*) Case (I) and $A = -1$.

(*c*)

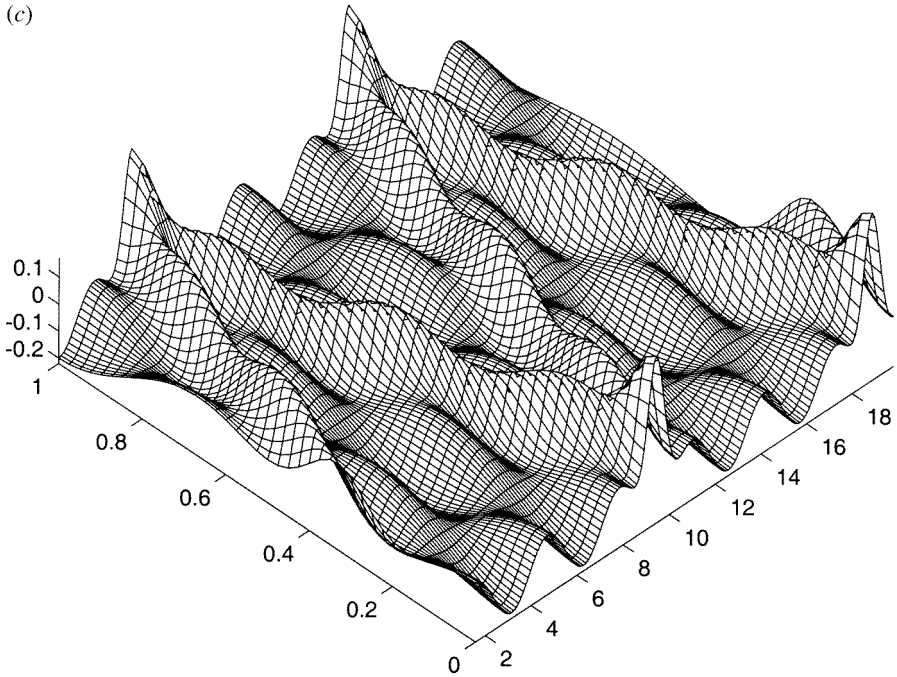

(*d*)

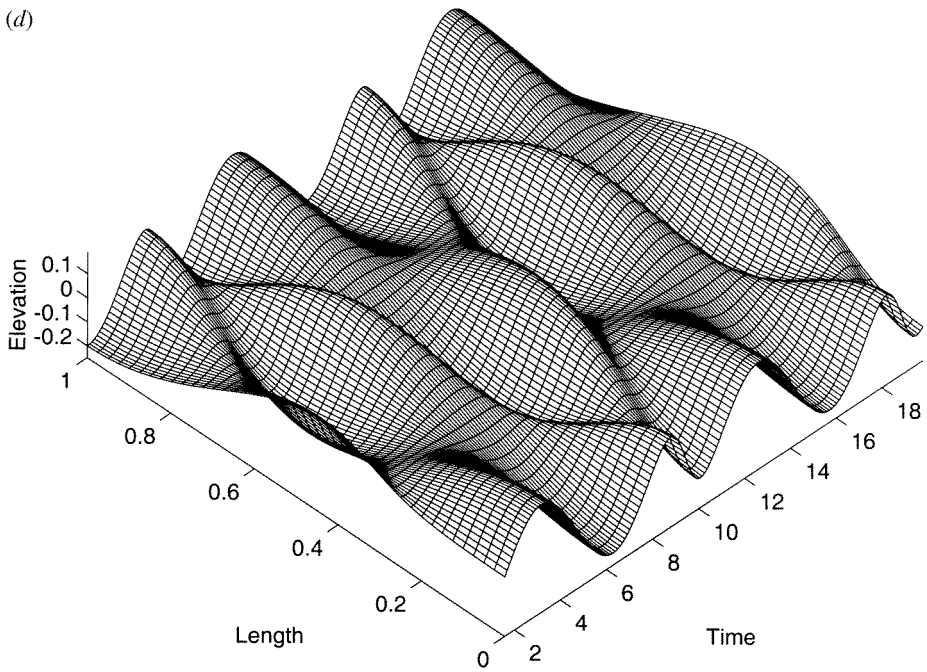

Figure 2. (Continued)

solution to (48) in the form

$$\Phi = A_1 + B_1 \sin^2 \omega_k(\tau - \Delta) \tag{49}$$

where $\Delta = \arcsin R$ [13]. Expression (49) is substituted into (48). Next, equating to zero the constant terms and the terms containing $\cos 2\omega_k(\tau - \Delta)$ we obtain two equations for unknown values B_1 and ω_k:

$$B_1 = (1 - A_1^2 + q_0 A_1)(A_1 - 0.5q_0)^{-1} \qquad \omega_k^2 = 0.5(A_1 q_0^{-1} - 0.5). \tag{50}$$

We assumed that $A_1 \gg B_1$ and neglected in (48) terms which had order B_1^2. We also assumed, defining ω_k^2, that $|q_0| \ll 1$. Expressions (50) are defined by unknown A_1. Let us find A_1 using solution (32). It follows from (32) and (49) that behind the front $A_1 \approx A + C$. According to the second scenario behind the front $A_1 \approx A - B$. The last case corresponds to waves considered in [13]. Now we can construct the approximate solutions which are valid at and behind the front. According to the first scenario

$$F'(\xi) = 2R\pi^{-1}\sqrt{\varepsilon} + A \tanh(e \sin M^{-1}\xi - eR) \cos \xi + [B \sec h^2(e \sin M^{-1}\xi - eR) + C] \times \cos^2 \xi + B_1 \sin^2 \omega_k(\tau - \Delta) \cos \xi H(\sin \xi - R). \tag{51}$$

Here

$$B_1 = [1 - (A + C)^2 + q_0(A + C)](A + C - 0.5q_0)^{-1} \qquad \omega_k^2 = 0.5[(A + C)q_0^{-1} - 0.5] \tag{52}$$

and H is the Heaviside function. According to the second scenario

$$F'(\xi) = 2R\pi^{-1}\sqrt{\varepsilon} + A \tanh(e \sin M^{-1}\xi - eR) \cos \xi - B \tanh^2(e \sin M^{-1}\xi - eR) \cos^2 \xi + B_1 \sin^2 \omega_k(\xi - \Delta) \cos \xi H(\sin \xi - R). \tag{53}$$

Here $B_1 = [1 - (A - B)^2 + q_0(A - B)](A - B - 0.5q_0)^{-1}$, $\omega_k^2 = 0.5[(A - B)q_0^{-1} - 0.5]$.

Solution (53) generalizes the results presented in [13]. However, in contrast with [13], here we did not take into account the viscous effect on the cnoidal-type waves. The last waves, as oscillations with a slowly varying mean value and an amplitude which is reduced to zero before the end of each cycle, were observed in [22]. Strictly speaking, solutions (51)–(53) are valid near the front when $R \ll 1$ and conditions (30) hold.

2.5. Free waves

According to quadratically nonlinear equation (26) the free oscillations are not generated in the system if $d = d_1 = 0$ [13, 24]. Here we consider the effect of the cubic nonlinearity on the free oscillations. For this case we have from (21) and (26) that

$$-D_1(F')^2 = F''' + D_2 F' + D_4 F'' + D_3(F')^3 - D \tag{54}$$

where $D_1 = -\beta/2k^*a_0$, $D_2 = -2\pi N(\omega_1 + \omega^*)a_0^3/k^*L\omega^2$, $D_3 = -(1.375\beta^2 a_0^{-3} + \beta_1 a_0^{-1})/k^*$, $D_4 = \mu^*/k^*$, and $D = (d_2 + d_1 + dL)a_0^3/k^*L$. Let the approximate solution of (54) be a sum of travelling waves:

$$F'(t \pm x a_0^{-1}) = A \tanh e(\sin M^{-1}\xi) \cos M^{-1}\xi + [B \sec h^2(e \sin M^{-1}\xi) + C] \cos^2 M^{-1}\xi \tag{55}$$

where A, B, C and e are unknown constants. Expression (55), where $x = L$, is substituted into (54). Next, equating to zero nonlocalized terms, and terms containing $\sec h^2(e \sin M^{-1}\xi)$, or $\sec h^4(e \sin M^{-1}\xi)$ or $\tanh(e \sin M^{-1}\xi)$ we obtain four equations. Then, following section 2.3, we find equations for A, B, C and e:

$$\begin{aligned} &-A^2(D_1 + 2.25CD_3) = CD_2 + 0.75C^2 D_1 + 0.625C^3 D_3 - 2D - 2CM^{-2} \\ &e^2 BM^{-2} = D_1(BC - A^2) + eAM^{-1}D_4 + BD_2 - D_3(1.5CA^2 - 9BC^2/8) - 2BM^{-2} \\ &BD_1/3 + D_3(B^2 + 3BC)/6 = 0 \\ &A^2 D_3 = 2(M^{-2} - D_2 - CD_1 - 9D_3C^2/8). \end{aligned} \tag{56}$$

Influences of nonlinearity, topography, dissipation and the initial displacement and stress. If the amplitude of the wave is small so that the cubic term in (54) is negligible, then system (56) yields $B = 0$ and $A = -eD_4M^{-1}D_1^{-1}$. Thus, the cnoidal-type waves are defined by (55) in the inviscid material if $D_4 = 0$, $D \neq 0$ and the cubic nonlinear effect is very small. Let topographic and initial-state effects be very small so that $D = 0$. Then $C = 0$. Consequently, the quadratically nonlinear free waves cannot exist in the initially flat and free layers of the inviscid materials [13, 24].

It follows from the last analysis that in the initially flat and free layers of the inviscid materials only the intensive nonlinear free waves may exist.

3. Forced and free waves (free boundaries)

We do not know of Faraday-type experiments with layers having free lateral boundaries. However, it is known that vertical-induced seismic waves amplify in elongated natural resonators. Sometimes these resonators may be considered as layers with free boundaries. Thus, Nature realizes the Faraday-type experiment with layers having free lateral boundaries.

Let us consider here two examples of these experiments. First, a hill of length $2L$ is considered. The undisturbed hill surface is $y = h(x)$. The bed of the hill is at $y = 0$. Let the hill geometry be symmetrical with respect to the vertical $x = 0$, and $y = h(0)$ is the highest point of the hill top. The slope of the hill top with respect to the bed of the hill is constant and very small ($h_x = \alpha \ll 1$). Lateral surfaces of the hill are perpendicular to the bed and located at $x = \pm L$. We assume that the width of the hill is large enough so that our one-dimensional model is valid.

Let the seismic-induced vertical acceleration may be approximated by a periodical law: $g_y = \delta \cos \omega t$ where $\delta \ll g_0$. The lateral surfaces of the hill are free. The hill is symmetrical, therefore the boundary conditions may be presented so that

$$u = 0 (x = 0) \qquad u_x = u_s - u_r = 0 \qquad (x = L). \tag{57}$$

The next example is a slightly sloping continental shelf ($h_x = \alpha \ll 1$). It is assumed that a coastal wall has a nonzero depth and there $u = 0$ ($x = 0$). At $x = L$ the shelf falls away rapidly into the deep ocean and $u_x = 0$. It is known that an average length of a shelf is approximately 200 km and the average depth is about 200 m. Very large earthquakes only have a meaning for the shelf when the free oscillations of the Earth are excited. The frequency of these oscillations may be close to the fundamental frequency of the shelf. This frequency can have a period of approximately an hour. Therefore, very long resonant water waves can be generated on the shelf. One can see that this last problem is identical to the problem formulated for the hill.

Let us consider the condition at $x = L$. It follows from (57) and (21) that

$$\begin{aligned}
&j_1' - J_1' + j_2' - J_2' + j_3' - J_3' - A_*[(J_1')^2 + (j_1')^2] + A_*(s - r)(J_1'J_1'' - j_1'j_1'') \\
&\quad +0.5a_0^{-2}(\mu J_1'' - \mu j_1'' + kJ_1'''' - kj_1'''') - 0.5La_0^{-3}(\mu J_1''' + \mu j_1''' + kJ_1''''' + kj_1''''') \\
&\quad -2A_*(J_1'J_2' + j_1'j_2') + A_*(r - s)(j_1''j_2' - J_1'J_2'') + 0.5a_*[j_1'(J_1')^2 \\
&\quad -J_1'(j_1')^2 + 2j_1'j_1''J_1 - 2J_1'J_1''j_1] + (b_* - 0.5A_*^2) \\
&\quad \times\left[J_1'(j_1')^2 - j_1'(J_1')^2 + j_1'' \int (J_1')^2 \,\mathrm{d}r - J_1'' \int (j_1')^2 \,\mathrm{d}s\right] \\
&\quad -(1.5c_* - A_*^2)[(j_1')^3 - (J_1')^3] \\
&\quad +2A_*^2L^2a_0^{-2}[j_1'''(j_1')^2 - J_1'''(J_1')^2 + 2j_1'(j_1'')^2 - 2J_1'(J_1'')^2] \\
&\quad -(2c_* - A_*^2)La_0^{-1}[j_1''(j_1')^2 + J_1''(J_1')^2] = 0.
\end{aligned} \tag{58}$$

We put $J_3 = J_3(r)$, $j_3 = j_3(s)$, and $d = d_1 = 0$. Functions $J_m(r)$ and $j_m(s)$ (here $m = 1$–3) are expressed by the Taylor's series, namely:

$$J_m(r) = F_{-m} + A_* u F'_{-m} + A_*^2 u^2 F''_{-m}/2 \ldots \qquad j_m(s) = F_{+m} - A_* u F'_{+m} + A_*^2 u^2 F''_{+m}/2 \ldots . \tag{59}$$

It is assumed that $J_m(t - xa_0^{-1}) = F_{-m}(t - xa_0^{-1} + La_0^{-1}) = F_{-m}$ and $j_m(t + xa_0^{-1}) = F_{+m}(t + xa_0^{-1} - La_0^{-1}) = F_{+m}$. In (59) we have

$$u = F_{-1} + F_{+1} + F_{-2} + F_{+2} + A_*(F_{-1} + F_{+1})(F'_{-1} - F'_{+1}) - A_* L[(F'_{-1})^2 + (F'_{+1})^2]/2 \ldots . \tag{60}$$

Using (59) and (60), and equating the terms of first, second and third order in (58) one can find that

$$\begin{aligned} &F'_{-1} = F'_{+1} = F',\ F'_{-2} = -A_*(F'_{-1})^2 - 2A_* F_{-1} F''_{-1} + \tfrac{1}{2}\mu a_0^{-2}(F''_{-1} - a_0^{-1} L F'''_{-1}) \\ &\qquad + \tfrac{1}{2} k a_0^{-2}(F'''_{-1} - a_0^{-1} L F''''_{-1}) \\ &F'_{+2} = A_*(F'_{+1})^2 + 2A_* F_{+1} F''_{+1} + \tfrac{1}{2}\mu a_0^{-2}(F''_{+1} + a_0^{-1} L F'''_{+1}) + \tfrac{1}{2} k a_0^{-2}(F'''_{+1} + a_0^{-1} L F''''_{+1}) \\ &F'_{-3} = -La_0^{-1}(2c_* + 7A_*^2) F''_{-1}(F'_{-1})^2 \qquad F'_{+3} = La_0^{-1}(2c_* + 7A_*^2) F''_{+1}(F'_{+1})^2 . \end{aligned} \tag{61}$$

Here, F' is an unknown function which is defined by the boundary condition (57) at $x = 0$. Let us consider the linear terms in this condition neglecting the dissipative effect. For this case

$$F(t \pm x/a_0) = l_*[(2 - k\omega^2 a_0^{-2}) \cos \omega L a_0^{-1} - kL\omega^3 a_0^{-3} \sin \omega L a_0^{-1}]^{-1} \cos \omega (t \pm x a_0^{-1}). \tag{62}$$

Here $l_* = -\alpha\delta\omega^{-2}$. Now the elevation and the horizontal acceleration may be calculated:

$$\begin{aligned} &\eta = h_0 a_0^{-1}[F'(r + La_0^{-1}) - F'(s - La_0^{-1})] \\ &u_{tt} = F''(r + La_0^{-1}) - F''(s - La_0^{-1}). \end{aligned} \tag{63}$$

The resonant frequencies are defined from (62) as

$$\Omega_N^* = \Omega_N - \Omega^* \qquad (N = 1, 2, 3, \ldots). \tag{64}$$

Here $\Omega_N = (N - 0.5)\pi a_0 L^{-1}$ and $\Omega^* = 0.5 k a_0 \pi^3 L^{-3}(N - 0.5)^3$.

3.1. Nonlinear, trans-resonant, dispersive and dissipative effects

Let us obtain an equation for F which is valid at and near the resonant frequencies (64). From (57) and (21) it follows that at $x = 0$ we have

$$\begin{aligned} &J_1 + j_1 + J_2 + j_2 + J_3 + j_3 + 0.5 a_*[j_1(J'_1)^2 + J_1(j'_1)^2] \\ &\qquad + (b_* - 0.5A_*^2)\left[J'_1 \int (j'_1)^2 \,\mathrm{d}s + j'_1 \int (J'_1)^2 \,\mathrm{d}r \right] = l_* \cos \omega t . \end{aligned} \tag{65}$$

Here, according to (59), (61) and since $u = l_* \cos \omega t$ is very small, we have $J_1 = J_1(r) \approx F(r)$ and $j_1 = j_1(s) \approx F(s)$. Generally speaking, one can seek the approximate harmonic solution of (65). However, in this paper we are interested in *unfamiliar* waves. Near and at the resonances (64) function F is expanded in Taylor's series at $x = 0$:

$$\begin{aligned} F(t - La_0^{-1}) &= F[t + La_0^{-1} - (2N - 1)\pi\omega^{-1} + 2\omega^{-1} a_0^{-1} L(\omega_1 + \Omega^*)] = -F(t + La_0^{-1}) \\ &\quad - \omega_* F'(t + La_0^{-1}) - 0.5\omega_*^2 F''(t + La_0^{-1}) - \omega_*^3 F'''(t + La_0^{-1})/6 \ldots \end{aligned} \tag{66}$$

It is assumed here that $\omega_* = 2\omega^{-1} a_0^{-1} L(\omega_1 + \Omega^*)$, $F[t + La_0^{-1} - (2N-1)\pi\omega^{-1}] = -F(t + La_0^{-1})$ and $\omega = \Omega_N^* - \omega_1$. Now the boundary condition (65) may be reduced, after using (59)–(61) and (66) to the basic equation:

$$-\omega_* F' - \mu_* a_0^{-3} L F'' - k_* a_0^{-3} L F'''' + \gamma (F')^3 = l_* \cos \omega t . \tag{67}$$

Here $\mu_* = \mu + 0.5L^{-1}\omega_*^2 a_0^3$, $k_* = k + L^{-1}\omega_*^3 a_0^3/6$, $\gamma = -0.67La_0^{-1}(2c_* + 7A_*^2)$ and $F = F(t + La_0^{-1})$. It should be emphasized that the dissipative and dispersive terms in (67) depend on ω. We now examine the nonlinear, trans-resonance, dissipative and dispersive effects on the solution of equation (67).

Nonlinear effect. If $\omega_* = k_* = \mu_* = 0$ we have

$$F'[t \pm (x - L - 0.25\beta u a_0^{-2})a_0^{-1}] = (l_*\gamma^{-1}\cos\omega\xi_*)^{1/3}. \tag{68}$$

Here $\xi_* = t \pm (x - L - 0.25\beta u a_0^{-2})a_0^{-1} \pm (N - 0.5)\pi\Omega_N^{-1}$. Thus, due to the nonlinear effect, the resonant oscillations have finite amplitude.

Trans-resonant effect, nondispersive medium. We rewrite equation (67) so that

$$Y^3 + (3R/2^{2/3})Y + \cos\omega t = 0 \tag{69}$$

where $Y = (-l_*^{-1}\gamma)^{1/3}F'$ and here $R = 2^{2/3}\omega_*(-l_*^{-1}\gamma)^{-1/3}/3$. In (69) R is a trans-resonant parameter. Solutions of (69) are defined by a value of R. If $R > 0$ there is the next real solution of (69):

$$Y = -2R_1\sinh(\varphi_*/3) \tag{70}$$

where $R_1 = 2^{-1/3}(\operatorname{sign}\cos\omega t)|R|^{0.5}$ and $\sinh\varphi_* = (\operatorname{sign}\cos\omega t)|R|^{-1.5}\cos\omega t$ and $\phi_* = \cos^{-1}|R|$. If $-1 \leqslant R < 0$ there is no continuous single-valued solution, and it is necessary to accept a solution with discontinuities. Following [25] we find that

$$Y = \begin{cases} -2R_1\cosh(\varphi_1/3) & \text{if } 0 < \omega t \leqslant \phi_* \quad \text{or} \quad \pi - \phi_* < \omega t \leqslant \pi + \phi_* \\ & \text{or} \quad 2\pi - \phi_* < \omega t \leqslant 2\pi \\ -2R_1\cos(\varphi_2/3) & \text{if } \phi_* < \omega t \leqslant \pi/2 \quad \text{or} \quad \pi + \phi_* < \omega t \leqslant 2\pi/3 \\ -2R_1\cos(\varphi_2/3 + 2\pi/3) & \text{if } \pi/2 < \omega t < \pi - \phi_* \quad \text{or} \quad 3\pi/2 < \omega t < 2\pi - \phi_*. \end{cases} \tag{71}$$

Here $\cosh\varphi_1 = (\operatorname{sign}\cos\omega t)|R|^{-1.5}\cos\omega t$, $\cos\varphi_2 = (\operatorname{sign}\cos\omega t)|R|^{-1.5}\cos\omega t$. If $R < -1$ there are three continuous real solutions of (69):

$$Y = -2R_1\cos[\phi_2/3 + 2(i_* - 1)\pi/3] \qquad i_* = 1, 2, 3. \tag{72}$$

It should be emphasized that there is also the acoustics solution. Linear (62), and nonlinear (70)–(72) solutions may describe different scenarios of the trans-resonant evolution of waves. It is important that the elevation is not symmetrical with respect to $R = 0$. In contrast to case $R \geqslant 0$, the surface discontinuities may be generated if $-1 < R < 0$ when

$$\omega t = n\pi - \phi_* \qquad n = 1, 2, 3, \ldots. \tag{73}$$

These discontinuities arise because of the simplification of equation (67).

Effect of weak dispersion. Let us return to equation (67) and take into account the dispersive effect for $-1 < R < 0 (\omega_* < 0)$. For a qualitative analysis it is assumed that an influence of the dispersion is accumulated at and near (73) and $|R| \ll 1 (\cos\omega t \approx 0)$. For this case equation (67) yields

$$K_*(F'')^2 = (F')^4/16 - 2\Omega(F')^2 + C_* \tag{74}$$

where $K_* = Lk_*\gamma^{-1}a_0^{-3}/8$, $\Omega = \omega_*\gamma^{-1}/16$ and C_* is an integration constant. Case $C_* = 16\Omega^2$ was considered in [12]. Let $C_* = 0$; then equation (74) is approximately satisfied if

$$F' = \sqrt{32\Omega}\sec h(\omega^{-1}\sqrt{-2\Omega/K_*}\cos\omega t)\sin\omega t. \tag{75}$$

It is assumed that $\omega^{-1}\sqrt{-2\Omega/K_*} \gg 1$. Using the expressions for Y and (75) we construct the expression for F' which is valid if the influence of the dispersion on equation (67) is small and localizes at and near (73):

$$F' = \sqrt{32\Omega}\Phi_*(t + La_0^{-1}) \sin \omega t + (-l_*\gamma^{-1})^{-1/3} Y[1 - \Phi_*^2(t + La_0^{-1})]. \quad (76)$$

Here $\Phi_*(t + La_0^{-1}) = \sec h(\omega^{-1}\sqrt{-2\Omega/K_*} \cos \omega t)$. Thus a smooth solution of equation (67) is constructed which is valid if $-1 < R < 0$. Solution (76) transforms to $F' = (-l_*\gamma^{-1})^{-1/3} Y$ if $|\cos \omega t|$ increases from zero.

Generally speaking, the first term in (76) may be very small. Now, using (76) and (63) we can write expressions for the resonant travelling waves. For example, for the travelling waves of the horizontal acceleration we have

$$\begin{aligned} F''[t \pm (x - L - 0.25\beta u a_0^{-2})a_0^{-1}] = {} & -8\Omega\sqrt{-K_*^{-1}} \sec h^2(\omega^{-1}\sqrt{-2\Omega K_*^{-1}} \cos \omega\xi_*) \\ & \times \sinh(\omega^{-1}\sqrt{-2\Omega K_*^{-1}} \cos \omega\xi_*) \sin^2 \omega\xi_* + (-l_*\gamma^{-1})^{-1/3} Y_t(\xi_*) \\ & \times [1 - \sinh^2(\omega^{-1}\sqrt{-2\Omega K_*^{-1}} \cos \omega\xi_*)]. \end{aligned} \quad (77)$$

The first term in (77) takes into account the dispersive effect which accumulates near lines where $\omega\xi_* = \pi n - \phi_*$.

3.2. Effect of strong dispersion and the localized solution

In this case we write equation (67) so that

$$F''' + D_2F' + D_4F'' + D_3(F')^3 - l^* \cos \omega t = 0 \quad (78)$$

where $D_2 = \omega_* a_0^3/k_*L$, $D_4 = \mu_* k_*^{-1}$, $D_3 = -\gamma a_0^3/k_*L$ and $l^* = -\alpha\delta a_0^3/k_*L\omega^2$. We assume the solution of (78) in the form

$$F'[t \pm (x - L - 0.25\beta u a_0^{-2})a_0^{-1}] = [B \sec h^2(e \sin M^{-1}\xi_* - eR) + C] \cos M^{-1}\xi_* \quad (79)$$

where B, C, e are unknown constants and $x = 0$. We shall assume that $\cos M^{-1}\xi_* = \cos \xi_*$ in (79). Expression (79) is substituted into (78). Next, equating to zero nonlocalized terms, and terms containing $\sec h^2(e \sin M^{-1}\tau - eR)$ or $\sec h^4(e \sin M^{-1}\tau - eR)$ we obtain three equations. Then, following section 2.3, we can find the following algebraic equations for B, C and e:

$$\begin{aligned} & D_2C - C + 0.5D_3C^3 - l^* = 0 \\ & Be^2M^{-2} + B - D_2B - 1.5D_3BC^2 = 0 \\ & 3C + B = 0. \end{aligned}$$

Thus $|B| \gg C$ and localized waves are defined by (79) if $e^2 \gg 1$. Recall that $M^{-1} = 1, 3, 5, \ldots$ according to section 2.3.

Free oscillations (trapped seismic waves). If $D_2 = l^* = 0$ then $C^2 = 2D_3^{-1}$, $e^2 = 2M^2$, and $B = -3C$ in (79). One can see that $|e| \gg 1$ only if $M = 3, 5, 7, \ldots$. Thus subharmonic (having low frequency) localized free waves may be excited in elongated topographies during earthquakes due to a sole shake according to the presented theory.

3.3. Earthquake-induced oscillations of the Tarzana hill as an example of the Faraday-type experiment in Nature

The Northridge 1994 Southern California earthquake caused extremely violent shaking at a site in Tarzana, California, located about 6 km south and 18.7 km about the mainshock

hypocentre. The peak horizontal acceleration ($1.78g_0$) was about a factor of ten higher than was observed at most other sites at an equal epicentral distance, and it was considerably higher than expected from empirical acceleration curves and numerical simulations [26–28]. In [28] it was emphasized that there was not an adequate explanation for the above violent shaking or why the 3.2 Hz resonance is strongest within 50 m of the hill top.

The Tarzana hill is 500 m long, 130 m wide, and reaches a maximum height of 20 m above the surrounding terrain. The shear-wave velocity under the hill is 369 m s^{-1}. We assume $a_s = 249$ m s^{-1} in the hill because of a strong impedance contrast between the hill and the bed [27].

Analytical analysis. We shall consider this elongated hill as a layer with slightly varying thickness and free ends. As a result, a behaviour of the hill is described by the theory of this section. According to (62) and (63) a peak of the surface motion is excited near the highest point ($x = 0$) of the hill at the resonance. This conclusion qualitatively agrees with the data which were recorded for the Tarzana hill [26–28]. The violent ground motion affected the top and the centre of the hill. Let us calculate the first resonant frequency of the hill using formula (64) which takes into account both the height (20 m) and the length of the hill. Many important characteristics can be understood through polarization analyses. According to [27] the largest ($L = 250$ m) and smallest ($L = 100$ m) dimensions of the hill are assumed. The dispersive effect we neglect ($k = 0$ in (64)). Then, for $L = 250$ m we have $\Omega_1 = 1.77$. This value correlates with frequency peak presented in figure 6 from [27]. For $L = 100$ m we have $\Omega_1 = 4.42$. The latter correlates with main frequency peak (3.26 Hz) presented in figure 6 from [27]. It is easy to find from (64) the dimension ($L = 139$ m) of the hill which corresponds to the main frequency peak. For this dimension (the dimension depends on the direction of measuring the hill) we have strong amplification which orients approximately perpendicular to the long axis of the hill. This result agrees with the observations [26–28]. The fundamental frequencies of the hill, corresponding to different L ($100 < L < 250$ m), range from 1.8 to 4.5 Hz. Thus one can see that formula (64) approximately describes some results of the calculations [26] and the observations [26–28].

In figures 3–5 nonlinear waves calculated for $L = 139$ m are presented. The length in figures 3–5 is related to L. The left-hand half of the hill is considered in figure 3 where a travelling wave of the horizontal acceleration is presented. We assumed $R = 0.3$ and $l_* = 0.00\,002$ m. A maximum amplitude of the acceleration peaks is at the centre ($x = 0$) of the hill, where peaks follow after craters and vice versa. This maximum reduces and the profile of the oscillations varies when x increases. At approximately $x = L/2$, oscillations are generated reminiscent of shock waves having two peaks. Thus, according to the theory, the largest resonant amplification of the horizontal accelerations takes place at the centre of the hill. This amplification may be very local.

Trans-resonant evolution of the surface waves in the Tarzana hill is shown in figure 4. We note that the curves in figure 4 qualitatively agree with experimental oscillograms of earthquake centrifuge modelling [29]. The sand was excited in the horizontal direction in a container for earthquake tests. The shaking was transient but its frequency ($\approx$1.9 Hz) was close to the fundamental frequency ($\approx$2.6 Hz) of the container. A shear deformation of the sand was maximum at the free surface and zero on the bottom. As a result, the upperlying layer and bottom layer of the sand had slightly different fundamental frequencies and R ($R < 0$). Travelling oscillons were excited during the experiments near the bottom while shock-like waves were excited near the free surface (see figures 14, 16, 18 and 21 from [29]). This effect may be explained by the influence of R according to figure 4. We simulated the Tarzana hill behaviour in point $x = 0.25L$ for different negative R and $l_* = 0.5 \times 10^{-5}$ m.

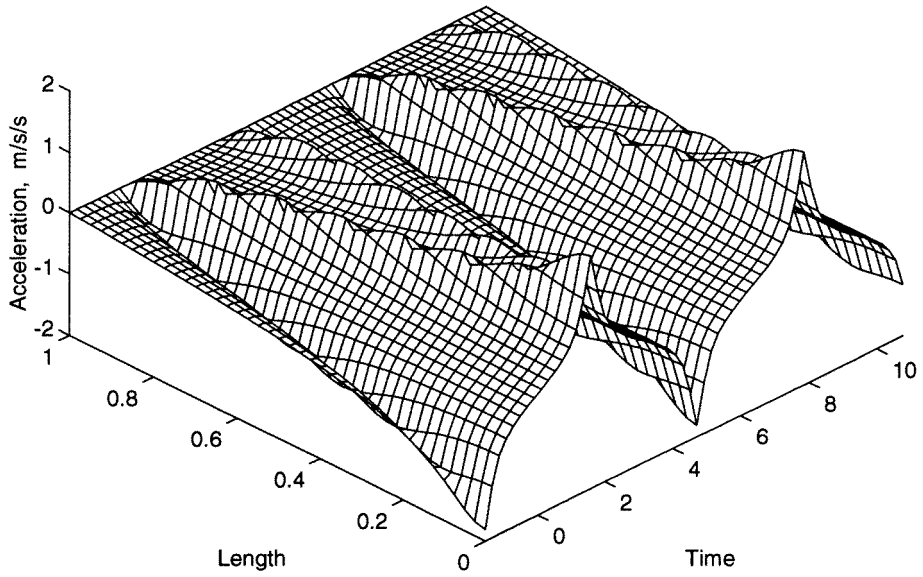

Figure 3. Travelling oscillon calculated according to (70) and (63) for $N = 1$.

The number of oscillons travelling up and down along the hill depends on the exciting frequency. These waves can form different patterns. Some of them, calculated according to (70) and (63) for $l_* = 0.000\,02$ m, are shown in figure 5 ($R = 0.05$ and $N = 3$). One can see that on the surface of the Tarzana hill the standing oscillons are formed as a result of a collision between the two travelling oscillons. The generation of these oscillons is similar to the generation of standing waves in linear acoustics but here we have the nonlinear effect and the standing oscillons may be very strongly located.

Since the earthquake-induced vertical acceleration of the hill was $1.15g_0$ [28], a tension zone could periodically generate near the base. There, a small gap could periodically generate. As a result of a periodical annihilation of this gap (periodical collisions of the hill with the bed) the strongly nonlinear waves had to be excited in the Tarzana hill. This amplification recalls an effect for a vertical water column which was experimentally studied by Natanzon [30].

Experimental and theoretical analysis of strongly nonlinear waves. The oscillations were excited by a piston at the bottom of the tube. The pressure on the free surface of the water column was equal to atmospheric pressure. The velocity of sound in the tube was 750 m s^{-1}. The radius was 12 cm; the length of the water column was varied from 4 to 7.5 m. Therefore, the fundamental frequency of the water column approximately changes from 300 to 160 Hz. In figures 6 and 7 oscillograms of the water pressure measured near the piston are presented. The sinusoidal curves show the piston position. During the experiments the excited frequency was increased slowly from 5 to 18 Hz and then was slowly reduced to 5 Hz. One can see that in the frequency range extending from 7.7 to 17 Hz there are large variations of the pressure waves. Shock-like waves were excited near the piston instead of the sinusoidal acoustic waves for all the above water columns when the piston acceleration exceeded g_0. If an excited amplitude of the piston was 0.002 m, then the shock-like waves had a frequency equal to the frequency of the piston (figure 6). When the amplitude of the excitation exceeded a critical value, subharmonic oscillations were generated in the tube (figure 7). It is surprising that the above amplification took place at all. Indeed, the excited frequencies were lower than the fundamental frequencies

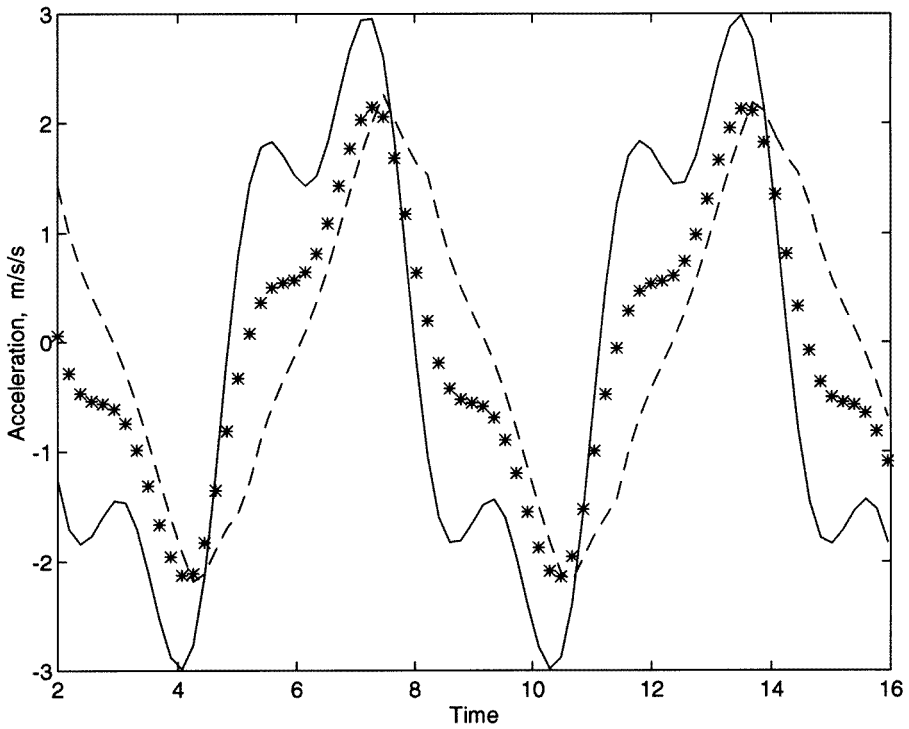

Figure 4. Trans-resonant curves of the acceleration calculated according to (77), $F''[t \pm (x - L - 0.25\beta u a_0^{-2})a_0^{-1}] = (-l_*\gamma^{-1})^{-1/3}Y_t(\xi_*) - 8\Omega\sqrt{-K_*^{-1}}\sinh(\omega^{-1}\sqrt{-2\Omega K_*^{-1}}\cos\omega\xi_*)\sin^2\omega\xi_*\sec h^2(\omega^{-1}\sqrt{-2\Omega K_*^{-1}}\cos\omega\xi_*)$ and (18) near the Tarzana hill top ($x = L/4$) for $R = -2$ (——), $R = -1.3$ (∗ ∗ ∗∗) and $R = -0.7$ (- - - -).

of the tubes by about ten times. Thus it was not the traditional resonance. The strong hysteretic effect is demonstrated in figure 6.

The results of numerical and analytical simulations of the above experiments were published [30, 31]. The strongly nonlinear state equation for the bubbly liquid, reminiscent of the state equation (8), was used in [31]. It was found that the amplification of the water wave was connected with the tension (cavitation) zone generated near the piston. We suggest that the same effect took place near the base of the Tarzana hill. Of course, vertical waves were excited in the tube while equation (13) was derived for horizontal waves. However, vertical waves in the Tarzana hill are also described by equation (13) and the boundary problem for these waves yields equation (67) [12]. Therefore, the Natanzon experiments describe both vertical and horizontal oscillations of the Tarzana hill. On the other hand, a very wide spectra of frequencies was generated because of the hill–base collisions [26].

In figures 8 and 9 the trans-resonant evolution of waves u_x in the top of the Tarzana hill is presented. The excited amplitude was 0.000 02 m, $L = 250$ m and $a_s = 249$ m s^{-1}. The excited frequency increases (figure 8) or decreases (figure 9) through resonant frequency Ω_1. The dashed curves in figure 8 were calculated according to acoustic solution (62). The other curves were calculated according to the nonlinear expressions (70)–(72). We emphasize that curves p and η are reminiscent of the curves in figures 8 and 9. One can see that the waves in figures 8 and 9 are an analogue of the strongly nonlinear pressure waves excited in the vertical

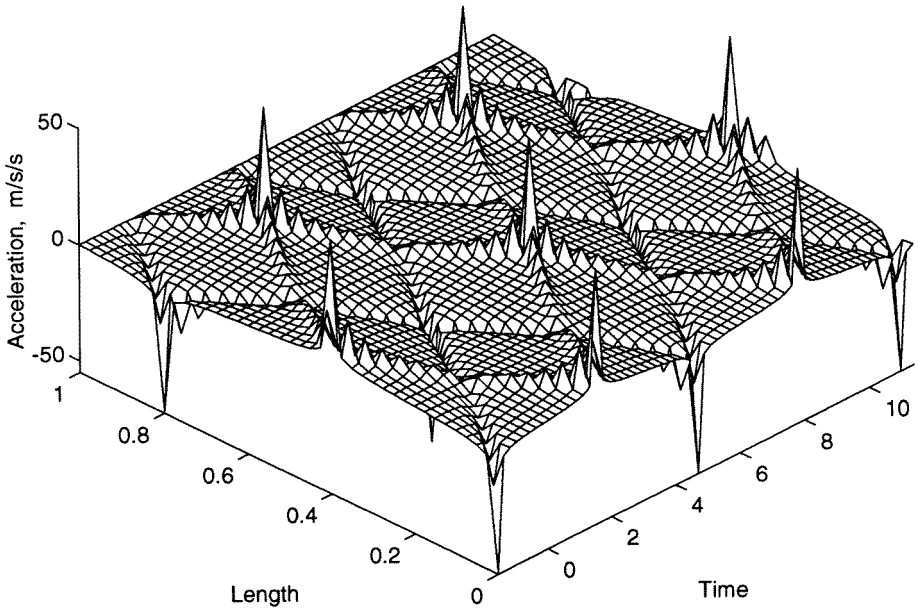

Figure 5. Localized oscillating excitations (standing oscillons) on the vibrated surface which are organized due to collisions of the travelling oscillons.

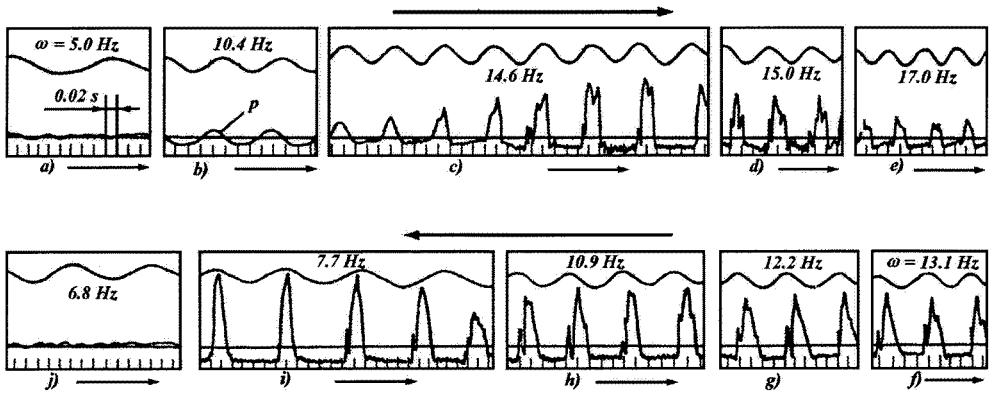

Figure 6. Hysteretic dynamics of strongly nonlinear oscillations of the water column (the exciting amplitude is 0.002 m and $L = 7$ m).

tube by the piston (figures 6 and 7). According to the theory and the calculations, the Tarzana hill demonstrates strongly hysteretic nonlinear behaviour during earthquakes.

Thus strongly nonlinear earthquake-induced seismic waves may be generated because of the topographic effect in natural resonators. On the other hand, these waves may be generated in the Faraday experiments with layers having free ends.

4. Unfamiliar parametric vertical-induced surface waves

Above we considered the case where $g_0 \gg g_y$. Let us now study cases when $g_0 \leqslant |g_y|$ or $g_0 \ll |g_y|$. Attention will be focused on limit cases when voidage $\phi_0 = 0$ (water waves) or

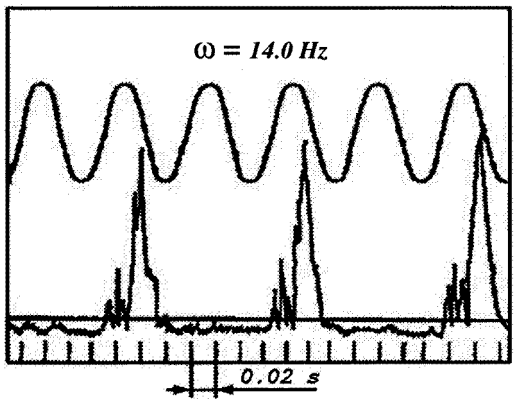

Figure 7. Subharmonic oscillations of the water column (the exciting amplitude is 0.004 m and $L =$ 6 m).

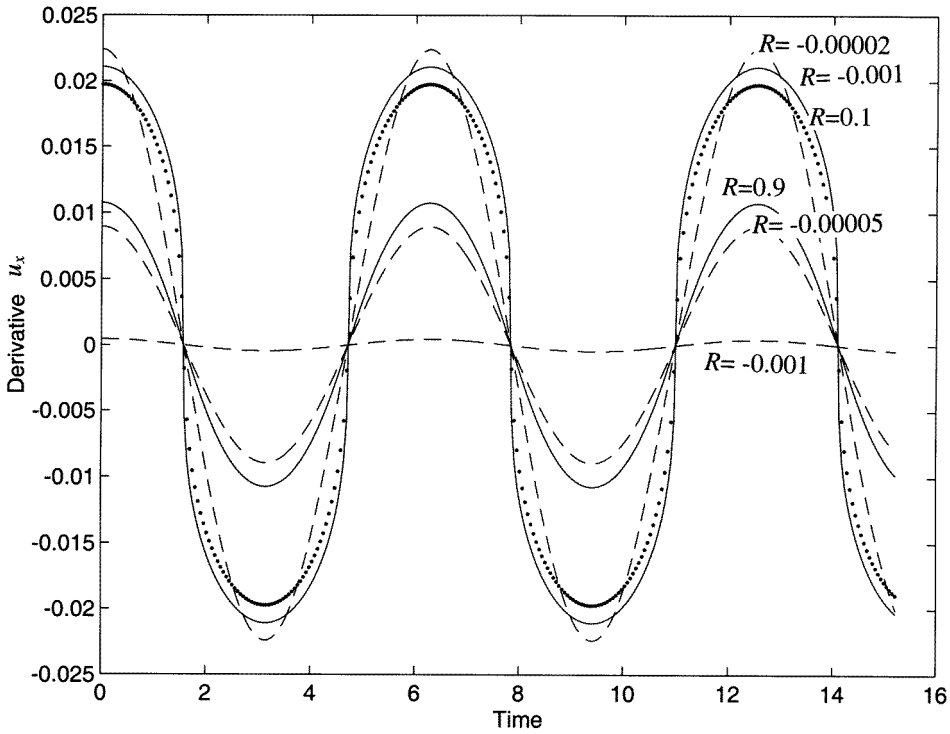

Figure 8. Hysteretic trans-resonant evolution of the Tarzana hill oscillations when the excited frequency increases.

$\phi_0\alpha_s = 1$ (granular waves). An equation for these cases follows from (13):

$$u_{tt} - a_0^2 u_{xx} = -gh_x - 3a_0^2 u_x u_{xx} + 6a_0^2 u_x^2 u_{xx} + \mu u_{txx} + \tfrac{1}{3}h_0^2 a_0^2 u_{xxxx} \tag{80}$$

where $a_0^2 = gh_0$. Equation (80) may be considered as a modification of Airy's equation [14] for nonlinear water waves. Thus we have here the perturbed nonlinear equation with the variable coefficients for dissipative–dispersive systems. We solve this equation following [24]. The free surface elevation η is defined so that

$$\eta = h(u_x^2 - u_x). \tag{81}$$

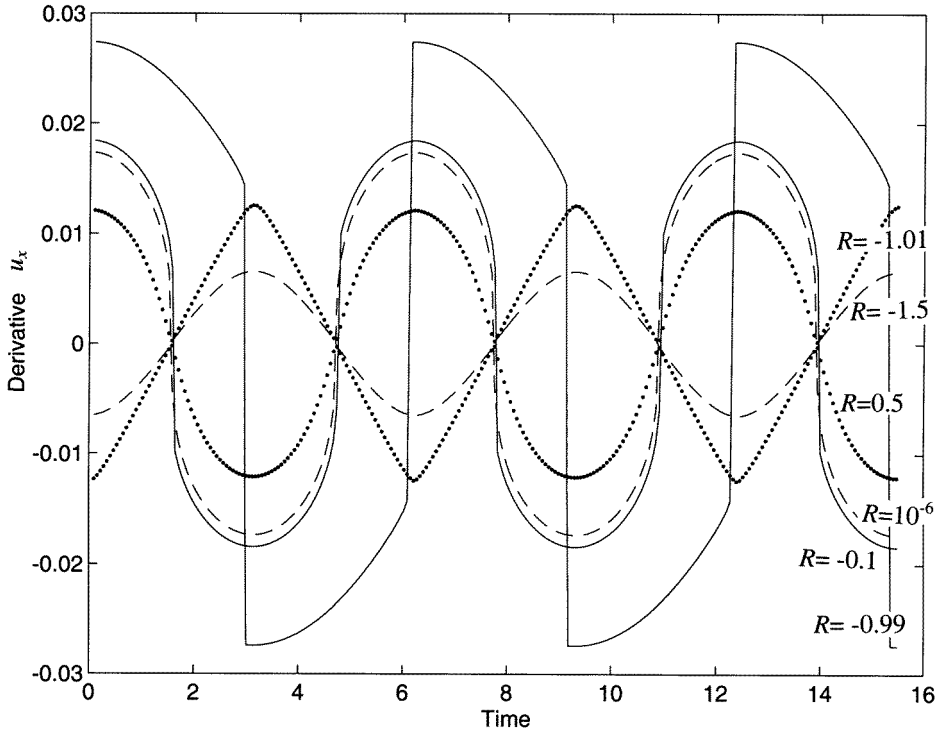

Figure 9. Hysteretic trans-resonant evolution of the Tarzana hill oscillations when the excited frequency decreases.

We shall seek a periodical solution of (80) that satisfies the next boundary conditions:

$$u = 0 \qquad \text{at} \quad x = 0 \quad \text{and} \quad x = L. \tag{82}$$

Analytical solutions are presented below, which explicitly demonstrate the influence of the amplitude of acceleration, and nonlinear, topographic, parametric, dispersive and dissipative effects on vertically induced surface water and granular waves.

4.1. Perturbation method

Equation (80) is rewritten, introducing the variables:

$$r = a(t) - x \qquad s = a(t) + x \tag{83}$$

where $a(t)$ is an unknown function which will be determined later. One can find that

$$u_x = u_s - u_r \qquad u_t = a_t(u_s + u_r) \qquad u_{xx} = u_{rr} - 2u_{rs} + u_{ss}$$

$$u_{tt} = (a_t)^2(u_{rr} + 2u_{rs} + u_{ss}) + a_{tt}(u_r + u_s) \qquad u_{xxxx} = u_{rrrr} - 2u_{rrss} + u_{ssss}$$

$$u_{txx} = a_t(u_{rrr} - u_{rss} - u_{rrs} + u_{sss}).$$

Here $a = a(t)$ and the subscripts r and s refer to partial derivatives with respect to r and s, respectively. Let $a_t^2 = a_0^2$. Then, neglecting terms of the fourth order, we rewrite equation (80) so that

$$\begin{aligned} 4a_0^2 u_{rs} = {} & -g(h_s - h_r) + 3a_0^2(1 + 2u_r - 2u_s)(u_r - u_s)(u_{rr} - 2u_{rs} + u_{ss}) \\ & + \mu a_t(u_{rrr} - u_{rss} - u_{rrs} + u_{sss}) + h_0^2 a_0^2(u_{rrrr} - 2u_{rrss} + u_{ssss})/3 \\ & - a_{tt}(u_s + u_r). \end{aligned} \tag{84}$$

The solution of (84) is presented as the sum $u = u_1+u_2+u_3$, where $u_1 \gg u_2 \gg u_3$. Substituting this sum into (84) and equating terms of the same order, one can obtain the following linear differential equations:

$$u_{1,rs} + 0.25a_{tt}a_0^{-2}(u_s + u_r) = 0 \tag{85}$$

$$4u_{2,rs} = -h_0^{-1}(h_s - h_r) - 3(u_{1,s} - u_{1,r})(u_{1,rr} - 2u_{1,rs} + u_{1,ss}) + \mu a_t^{-1}(u_{1,rrr} - u_{1,rss} - u_{1,rrs} + u_{sss}) + h_0^2(u_{1,rrrr} - 2u_{1,rrss} + u_{1,ssss})/3 \tag{86}$$

$$4u_{3,rs} = -3(u_{2,s} - u_{2,r})(u_{1,rr} - 2u_{1,rs} + u_{1,ss}) - 3(u_{1,s} - u_{1,r})(u_{2,rr} - 2u_{2,rs} + u_{2,ss}) + 6(u_{1,r} - u_{1,s})^2(u_{1,rr} - 2u_{1,rs} + u_{1,ss}). \tag{87}$$

Let the approximate solution of equation (85) be

$$u_1 = J(r) - J(s). \tag{88}$$

In this case equation (85) yields $-J'(s) + J'(r) = 0$. Let us assume that

$$J'(a + L) = J'(a - L). \tag{89}$$

Thus J' is the periodical function. One can see that equation (85) is satisfied approximately by (88) in case (89) near the boundaries. On the other hand, solution (88) is valid if $a_{tt}a^{-2} \approx 0$. Solution (88) is reminiscent of the d'Alembert-type solution (19), but here the velocity of waves $J(a \pm t)$ is not constant and depends on g_y. In particular, according to solution (88), standing or spatially oscillating or one-hand side travelling waves may be in vertical-induced layers [24]. Now we shall correct solution (88) taking into account u_2 and u_3. The wave-type solution of (86) is given by

$$u_2 = J_2(r) + j_2(s) - \tfrac{3}{8}\{r[J'(s)]^2 - s[J'(r)]^2 - 2J(s)J'(r) + 2J'(s)J(r)\} - 0.25\iint\{h_0^{-1}(h_s - h_r) - \mu a_t^{-1}[J''(r - J''(s)]\}\,\mathrm{d}r\,\mathrm{d}s + \tfrac{1}{12}h_0^2[sJ'''(r) - rJ'''(s)] + xd + d_1. \tag{90}$$

The prime denotes here the differentiation with respect to the appropriate variable (83). Let us assume that coefficient μ in (13) and (90) is a function of the vertical acceleration of the layer and

$$\eta^* = \eta_* a_t \tag{91}$$

where η_* is constant. Generally speaking, the expression (90) can contain secular terms. The secular terms will be eliminated if

$$J_2(r) = -3r(J')^2/8 - h_0^2 rJ'''/12 - \eta_* rJ''/4 + \alpha h_0^{-1}r^2/8 + \Psi_2(r)$$
$$j_2(s) = 3s(j')^2/8 - h_0^2 sj'''/12 - \eta_* sj''/4 + \alpha h_0^{-1}s^2/8 + \psi_2(s).$$

Here $J = J(r)$, $j = -J(s)$. For simplicity we will consider here layers with the thickness varying according to the linear law ($h_x = \alpha$, where α is constant). As a result we have the next expression for solution (90) which is valid near the boundaries or if (89) holds:

$$u_2 = \Psi_2(r) + \psi_2(s) + 0.375(s - r)[(J')^2 + (j')^2] - 0.75(jJ' - j'J) + (s - r)[h_0^2(J''' - j''') + 3\eta_*(J'' - j'') + 6d]/12 + 0.125\alpha h_0^{-1}(s - r)^2 + d_1. \tag{92}$$

We shall not take into account the influence of d and d_1 on the third-order values.

Using the expressions for u_1 (88) and u_2 (92) one can rewrite equation (87) so that

$$u_{3,rs} = 9\{0.5(j^2)'J''' + 0.5(J^2)'j''' - Jj'j''' - jJ'J''' - 3.5(j')^2J'' - 3.5(J')^2j'' + 3.5[(J')^2]'j' + 3.5[(j')^2]'J' - 5[(j')^3]/6 - 5[(J')^3]'/6 - JJ''j'' - jj''J'' - j(J'')^2 - J(j'')^2\}/16 - 9(s - r)\{j'[(J')^2]'' - J'[(j')^2]'' + J''[(j')^2]'$$

$$-j''[(J')^2]' + 2[(j')^3]''/3 - 2[(J')^3]''/3\}/32 + 1.5[J''(j')^2 - 2J'j'J''$$
$$+J''(J')^2 + j''(j')^2 - 2J'j'j'' + j''(J')^2] + 0.75[(\Psi_2'' + \psi_2'')(j' - J')$$
$$-(\Psi_2' - \psi_2')(J'' + j'')].$$

Here $\Psi_2 = \Psi_2(r)$, $\psi_2 = \psi_2(s)$. Now, after some algebra, one can find

$$u_3 = J_3(r) + j_3(s) + 9(J''j^2 + j''J^2)/32 - 9j'J'(J + j)/16 - 3[j(J')^2 + J(j')^2]/32$$
$$+3\left(j'\int (J')^2\,\mathrm{d}r + J'\int (j')^2\,\mathrm{d}s\right) + 7[s(J')^3 + r(j')^3]/32$$
$$+9(r - s)[2jJ'J'' - 2Jj'j'' + J'(j')^2 - j'(J')^2]/32$$
$$+9(s^2 - 2rs)J''(J')^2/32 + 9(r^2 - 2rs)j''(j')^2/32$$
$$+0.75\int\int [(\Psi_2'' + \psi_2'')(j' - J') - (\Psi_2' - \psi_2')(J'' + j'')\,\mathrm{d}r\,\mathrm{d}s. \tag{93}$$

We used in (93) that

$$\int\int (s - r)[(j')^3]''\,\mathrm{d}r\,\mathrm{d}s = 1.5(sr - 0.5r^2)j'[(j')^2]' - r(j')^3.$$

The secular terms are eliminated in (93) if

$$J_3(r) = \Psi_3(r) - 7r(J')^3/32 + 9r^2J''(J')^2/32$$
$$j_3(s) = \psi_3(s) - 7s(j')^3/32 + 9s^2j''(j')^2/32.$$

As a result we have the next expression for the displacement which is valid near the fixed boundaries:

$$u = J + j + \Psi_2(r) + \psi_2(s) + 0.75x(J')^2 + 0.75x(j')^2 - 0.75(jJ' - j'J)$$
$$+x[h_0^2(J''' - j''') + 3\eta_*(J'' - j'')]/6 + 0.5\alpha h_0^{-1}x^2 + xd + d_1 + \Psi_3(r) + \psi_3(s)$$
$$+9(J''j^2 + j''J^2)/32 - 9j'J'(J + j)/16 - 3[j(J')^2 + J(j')^2]/32$$
$$+3\left[j'\int (J')^2\,\mathrm{d}r + J'\int (j')^2\,\mathrm{d}s\right] + 7x[(J')^3 - (j')^3]/16$$
$$-9x[2jJ'J'' - 2Jj'j'' + J'(j')^2 - j'(J')^2]/16 + 9x^2J''(J')^2/8$$
$$+9x^2j''(j')^2/8 + 0.75\int\int [(\Psi_2'' + \psi_2'')(j' - J') - (\Psi_2' - \psi_2')(J'' + j'')]\,\mathrm{d}r\,\mathrm{d}s. \tag{94}$$

The boundary condition (82) at $x = 0$ is satisfied by (94) if we assume that

$$\Psi_2(r) = \psi_2(s) = -0.5d_1 \qquad \Psi_3(r) = \psi_3(s) = 0. \tag{95}$$

4.2. Viscous, nonlinear and topographic effects

Because of (89) expressions (94), (95) and the boundary condition (82) at $x = L$ yield the next equation:

$$-L(J')^3/4 + 2.25LJJ'J'' + 1.5L(J')^2 + h_0^2LJ'''/3 + \eta_*LJ'' + 0.5\alpha h_0^{-1}L^2 + Ld = 0 \tag{96}$$

where $J' = J'(a - L)$. Let J be the fast-varying function and $|J| \ll |J'|$. For this case the following coefficients are introduced:

$$D_1 = -4.5h_0^{-2} \qquad D_3 = -3/4h_0^2 \qquad D_4 = 3\eta_*h_0^{-2} \qquad D = -(1.5\alpha Lh_0^{-1} + 3d)h_0^{-2}. \tag{97}$$

As a result, equation (96) transforms into equation (54). Following section 2.5 we write the following expression for J':

$$J'(a \pm x) = A\tanh e(\sin M^{-1}\zeta - R)\cos M^{-1}\zeta$$
$$+[B\sec h^2(e\sin M^{-1}\zeta - R) + C]\cos^2 M^{-1}\zeta \tag{98}$$

where $\zeta = \pi L^{-1}(a \pm x + c_{\pm})$, A, B, C, e are unknown constants and R is the trans-resonant parameter. Values $c_{\pm}$ and M will be determined later. Let us assume that $|e| \gg 1$. Thus only localized waves are considered. These waves are localized near lines where $\sin \pi L^{-1} M^{-1}(a \pm x + c_{\pm}) \approx R$. In this case A, B, C, e are defined by system (56) where $D_2 = 0$ and M^{-2} is replaced by $\pi^2 L^{-2} M^{-2}$.

Influences of quadratic nonlinearity, dissipation, topography, and the initial state. If the amplitude of the wave is small so that the cubic term in (96) is negligible, then system (96) yields $B = 0$ and

$$A^2 = -0.5C^2 + DD_1^{-1} \qquad e = AD_1LM/\pi D_4 \qquad C = \pi^2 L^{-2} M^{-2} D_1^{-1}. \tag{99}$$

One can see from (99) that effects of the dissipation and D may be very important.

Discontinuous oscillations may generate in the inviscid system ($D_4 = 0$). Due to the weak dissipation the continuous shock-like parametric surface waves may be in layers. These waves were observed recently in granular layers [32]. At the same time, no oscillations are possible in the initially flat and free layers ($D = 0$) according to system (99). This result agrees with the conclusions of section 2.5.

4.3. Simulation of observed parametric water and granular waves

Generally speaking, the presented theory is valid for any excitation when $a_0 = \sqrt{g_0 h_0 + g_y h_0}$ is real [24]. However, in order to illustrate the theory we shall consider a one-frequency periodical oscillation of the bed according to sinusoidal law. If the amplitude of the exciting acceleration of the bed is small enough then we can suggest that in (13)

$$g_y = \delta \cos \omega t. \tag{100}$$

This case for water waves and $\delta = g_0$ was considered in [24]. Thus for water waves $a_t^2 = a_0^2 = g_0 h_0(1 + g_y g_0^{-1}) = g_0 h_0(1 + \delta g_0^{-1} \cos \omega t)$, and

$$a = (g_0 h_0)^{0.5} \int (1 + \delta g_0^{-1} \cos \omega t)^{0.5} \, \mathrm{d}t = (8 g_0 h_0 \omega^{-2})^{0.5} \sin \omega t/2. \tag{101}$$

If $\delta < g_0$, then according to (101)

$a = a(t) \approx \sqrt{h_0 g_0}(t + \frac{1}{2}\delta\omega^{-1} g_0^{-1} \sin \omega t - \frac{1}{16}\delta^2 g_0^{-2} t - \frac{1}{32}\delta^2 \omega^{-1} g_0^{-2} \sin 2\omega t \ldots)$.

One can see that the convergence of this series depends on ω. If ω is small then the series converges slowly. As a result, many harmonics may be generated in the system and the motion of the waves may be very complex. Apparently, the system moves to chaos when ω reduces while δ is close to g_0.

In contrast with the water waves, the granular waves are excited in experiments if $|g_y| > g_0$. If $\delta > 2g_0$ then the gas volume increases above some critical level and the thin granular layer loses the compact state. We shall simulate the surface waves for this case, suggesting that the vertical acceleration of the layer is a fast-varying function during the collision, contact and separation phase. Let a periodical excitation acting on the layer be

$$g_y = \delta_* \cos^n m^{-1} \omega t \tag{102}$$

where δ_* is an unknown constant, and here $n = 2, 4, 6, 8, \ldots$ and $m = 1, 2, 3, \ldots$. The constants δ_*, n and m may be defined from experiments [33]. In (102), degree n is defined by the intensity of the excitation and the contact time. Coefficient δ_* is defined by a velocity of a layer–bed collision. Coefficient m is defined by the flying time. Of course, the constants in (102) are defined by the excitation; however, we emphasize that (102) is not the acceleration of the bed. Expression (102) defines the acceleration of the layer, which is quite different from

the sinusoidal acceleration of the bed. In particular, (102) defines subharmonic oscillations excited by the sinusoidal acceleration of the bed if $m = 2, 3, \ldots$. Let δ_* be large enough so that we can neglect by the effect of the acceleration of gravity $|g_y| \gg g_0$. Due to the above assumptions, we may use equation (13) for the study of the nonlinear behaviour of the thin fluidized granular layers if there $a_0^2 = \delta_* h_0 \cos^n m^{-1}\omega t$. Thus $a = (\delta_* h_0)^{0.5} \int \cos^{n/2} m^{-1}\omega t \, \mathrm{d}t$ for the granular waves.

Solution (98) describes the rich variety of wave processes in water and granular layers. Therefore, we must extract questions of our interest for calculations. Let us focus our attention on wave patterns observed recently in water [34] and granular layers [6, 8, 32, 33, 35]. These patterns were simulated successfully with the help of numerical methods (see, for example, [8, 9, 33–35]). Here we use the analytical solutions.

Results of calculations of the wave patterns are given in figures 10–12, where the dimensionless coordinate (x/m) is used. The boundary friction (91) may be very important for the waves excited in these experiments. However, we do not know the friction parameters. Therefore, we will qualitatively simulate experimental results assuming, following [24], that $A = 0$, and $B = 1.8$, $C = -0.9$ $e \approx 1.423\pi^{-1}h_0^{-1}L$ in (98) (see also [36]).

Analysis of water wave experiments [34]. The rectangular tank was vertically vibrated in [34]. The tank was 0.2 m long and 0.025 m wide. The water depth h_0 was 0.02 m. Thus, the boundary friction may be very important for the waves excited in this experiment. We assumed that the bottom friction effect reduces the amplitude of water waves. Therefore, so as to roughly take this effect into account, we assume that $h_0 = 0.0066$ m in the calculations. Then we suggest that some wave patterns in the experiments were formed by the wave

$$u_x = -f_x(a + x) = -\{1.8 \sec h^2[1.423\pi h_0^{-1} L \sin \pi L^{-1} M^{-1}(a + x + c_+)] - 0.9\} \times \cos^2 \pi L^{-1} M^{-1}(a + x + c_+). \tag{103}$$

Results of the calculations for $\delta = g_0$, different M^{-1} and $c_\pm$ are presented in figure 10. We used (81), (101) and assumed that $\omega = 63$ Hz. These results correspond to the waves presented in figures 2(a), 1(a) and 3(a) from [34].

The double solitons (see figure 10(a)) were calculated according to (88) and (103) where $M^{-1} = 2$ and $c_+ = 0.75L$. These solutions are also presented in figure 2(a) of [34]. The double solitons, shown in figure 1(a) of [34], oscillate symmetrically with respect to the centre of the tank. We obtained these waves with the help of (88) and (98), assuming $M^{-1} = 2$, $c_- = -1.25L$, and $c_+ = 0.75L$. Figure 10(c) shows interactions and motions of the four solitons. We calculated these solitons assuming $M^{-1} = 4$, $c_- = -7L/8$, and $c_+ = 5L/8$. Thus figure 10 shows, qualitatively, interactions and motions of the solitons presented in [34].

Thus, using M^{-1} and constants $c_\pm$, we simulated qualitatively the experimental results for the water waves.

Simulation of granular-wave experiments [8, 33, 34]. Theoretical results calculated for $h_0/L = 0.05$, $L = 1$ m, $m = 2$, $c_\pm = L/4$, $\delta_* = 2.5g_0$ and $a = (\delta_* h_0)^{0.5} m\omega^{-1}(\sin m^{-1}\omega t - 0.333 \sin^3 m^{-1}\omega t)$, according to (102), (98), (88) and (81), are illustrated by figures 11 and 12. Figure 11 shows oscillons calculated for $\omega = 25$ Hz. Figure 12 presents wave patterns calculated for different ω: $\omega = 15$ Hz (a), $\omega = 7$ Hz (b), $\omega = 5$ Hz (c).

One can see in figure 11 the granular waves spatially oscillating with a small amplitude. The oscillons are a result of the focusing of these waves. The oscillons can form chains (see figures 11(a) and 12(a)). Perhaps these chains correspond to the so-called oscillon 'molecules' presented in figures 3(c) and (d) of [8]. If the excited frequency reduces then the chains begin to interact. This interaction and an influence of the boundaries give the hexagon-like

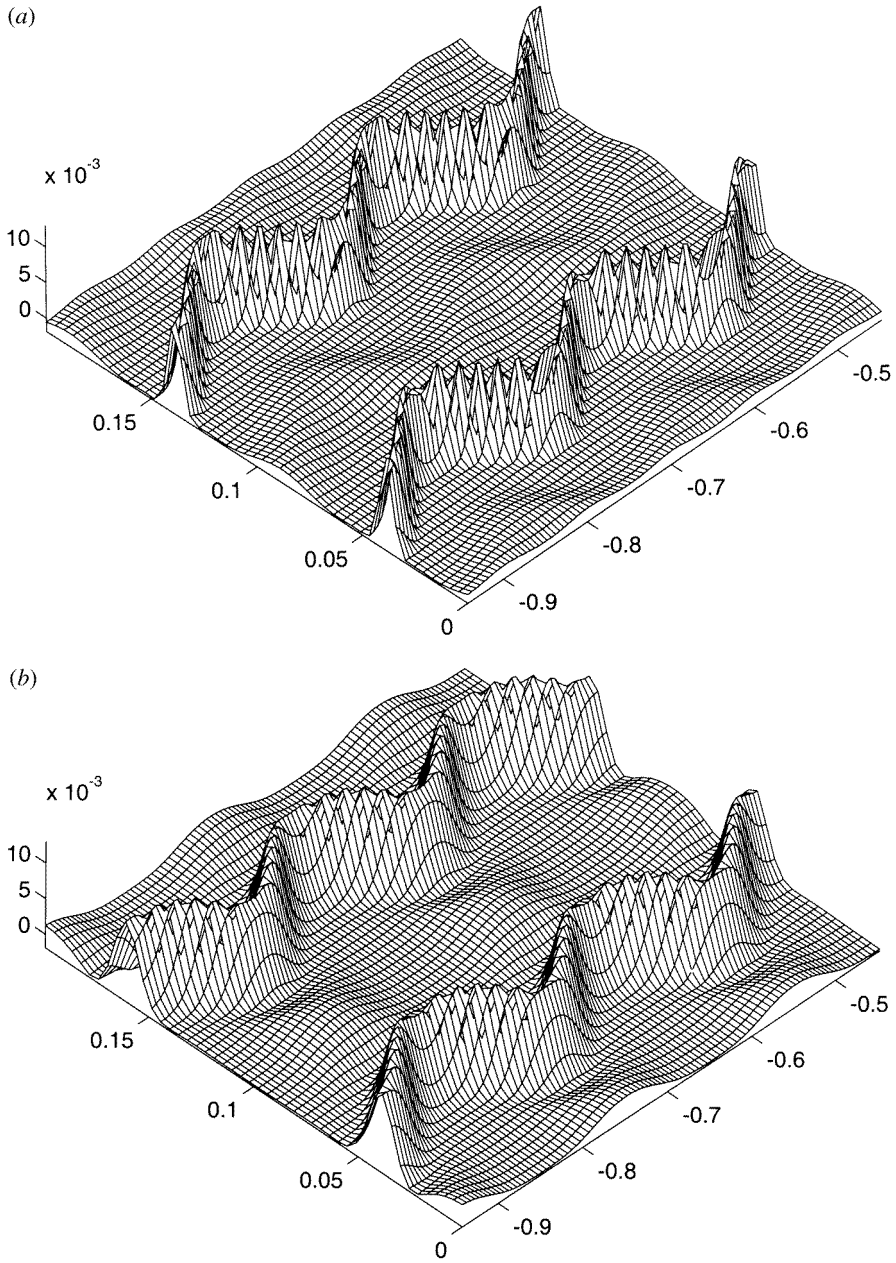

Figure 10. Stripe-like patterns on water surface.

pattern (figure 12(*b*)). Hexagonal patterns have been observed in different experiments (see, for example, [8, 35]). The rectangular-like patterns are shown in figure 12(*c*). Calculations showed that the square-, hexagon- and rectangular-like patterns may be forced for different n, layers and excitations. Indeed, square patterns as well as hexagonal pattern were often observed in experiments. These patterns can form the different nets in the x–t plane. Striped patterns are described with the help of (103). Perhaps the stripes observed in [33, 35] are a

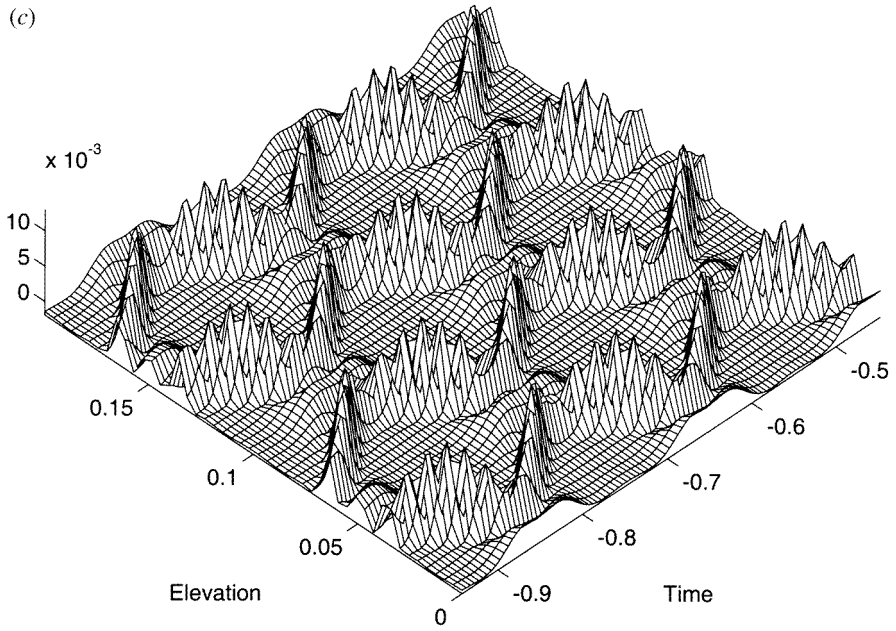

Figure 10. (Continued)

result of the excitation of one-hand side travelling oscillating waves (103).

The other wave patterns described by solution (98) are discussed in [24, 36].

4.4. Standing and arch parametric waves in deep granular beds

Spatially slowly varying waves were observed in [37, 38]. Let us assume that the generation of these waves is defined by an initial topography of the layer. It is suggested that $h_x = \sum_i H_i \sin 2\pi i x/L$ and $u = \sum_i U_i(t) \sin 2\pi i x L^{-1}$ in (80). Then, following [24], we obtain from (80) the next set of approximate independent equations:

$$U_i'' + 4\mu\pi^2 i^2 L^{-2} U_i' + gH_i + 4h(g_0 + g_y)\pi^2 i^2 L^{-2}(1 - 4h^2\pi^2 i^2 L^{-2}/3)U_i = -24h(g_0 + g_y)\pi^4 i^4 L^{-4} U_i^3. \tag{104}$$

We assume that

$$U_i = A_i \cos \omega t/2 + C_i. \tag{105}$$

Small-amplitude surface waves [38]. If the flying time is much smaller than the excitation period, we can suggest that $n = 1$ and $m = 1$ in (102), and therefore $g_y = \delta_* \cos \omega t$. Using the last expression and (104) we obtain the following equations:

$$C_i^3 = C_i[h^2/4.5 - i^{-2}\pi^{-2}L^2/6 - 0.75(2 + \delta_* g_0^{-1})A_i^2] - H_i h^{-1} i^{-4}\pi^{-4}L^4/24 \tag{106}$$

$$A_i[-0.25\omega^2 + 4hi^2\pi^2 L^{-2}(g_0 + 0.5\delta_*)(1 - 4h^2 i^2\pi^2 L^{-2}/3)] = -24A_i h i^4 \pi^4 L^{-4}[(0.75g_0 + 0.5\delta_*)A_i^2 + 3(g_0 + 0.5\delta_*)C_i^2]. \tag{107}$$

For a limit case $H_i \approx C_i \approx 0$ we have $A_i^2 = h^{-1} i^{-4}\pi^{-4} L^4 (18g_0 + 12\delta_*)^{-1}[0.25\omega^2 - 4hi^2\pi^2 L^{-2}(g_0 + 0.5\delta_*)(1 - 4h^2 i^2\pi^2 L^{-2}/3)]$. According to this case the subharmonic parametric standing waves

$$u = \sum_i A_i \cos(\omega t/2) \sin 2\pi i x L^{-1} \tag{108}$$

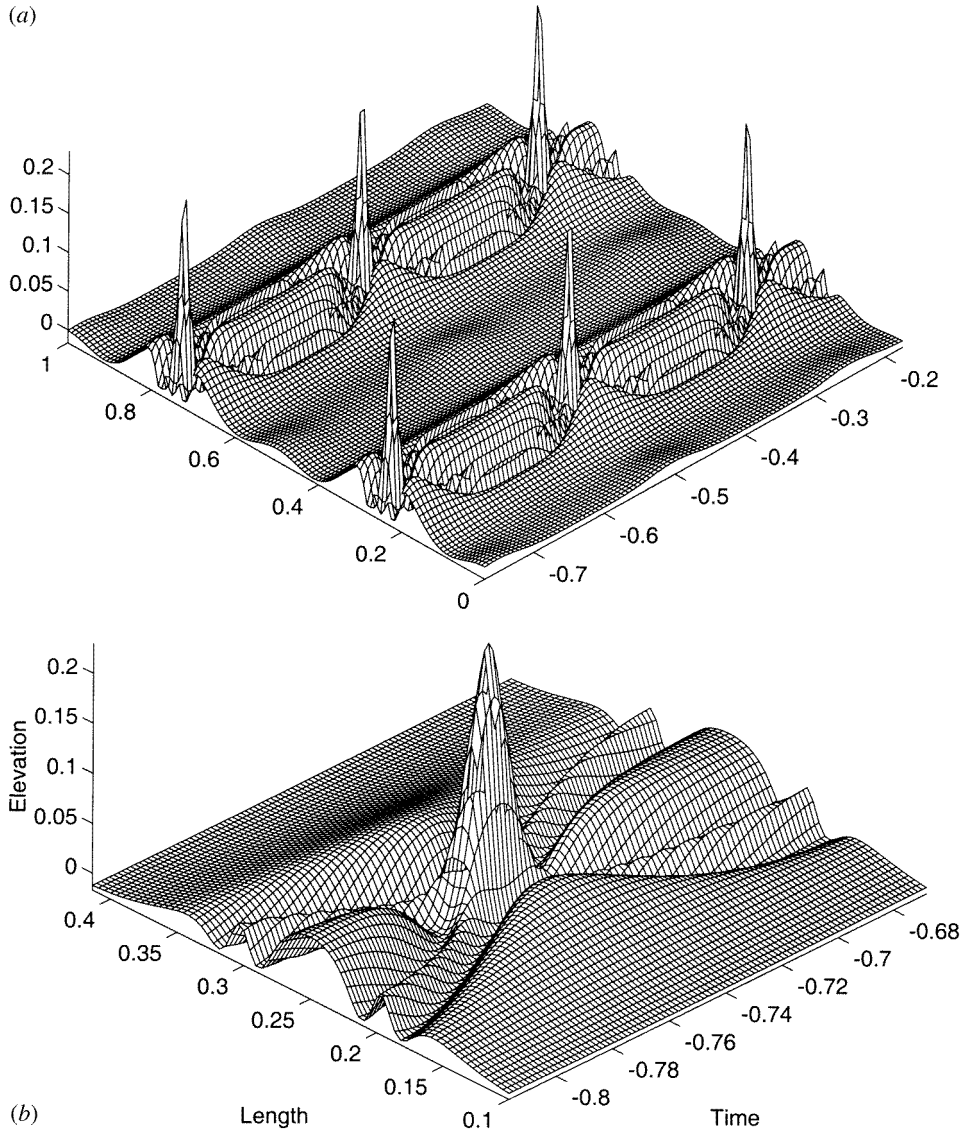

Figure 11. Stripe-like pattern is formed by oscillons (*a*) and dynamics of oscillon (*b*).

may be generated in the layer. These slowly varying waves exist if the excitation is intensive enough so that the cubic term in (13) begins to be important. This result agrees qualitatively with experiments. Indeed, the slowly varying granular waves were observed when the excited acceleration was increased above $2.2g_0$ [38].

Arch waves. If the excitation is increased then the flying and contact times of the deep bed may be comparable. In this case, $g_y = \delta_* \cos^2 \omega t$ (102) and

$$C_{i\pm} = \pm(h^2/4.5 - i^{-2}\pi^{-2}L^2/6 - 1.5A_i^2)^{0.5}$$
$$A_i^2 = -h^{-1}i^{-4}\pi^{-4}L^4(90g_0 + 43.5\delta_*)^{-1}[0.25\omega^2 + 8hi^2\pi^2L^{-2}(g_0 + 0.5\delta_*)$$

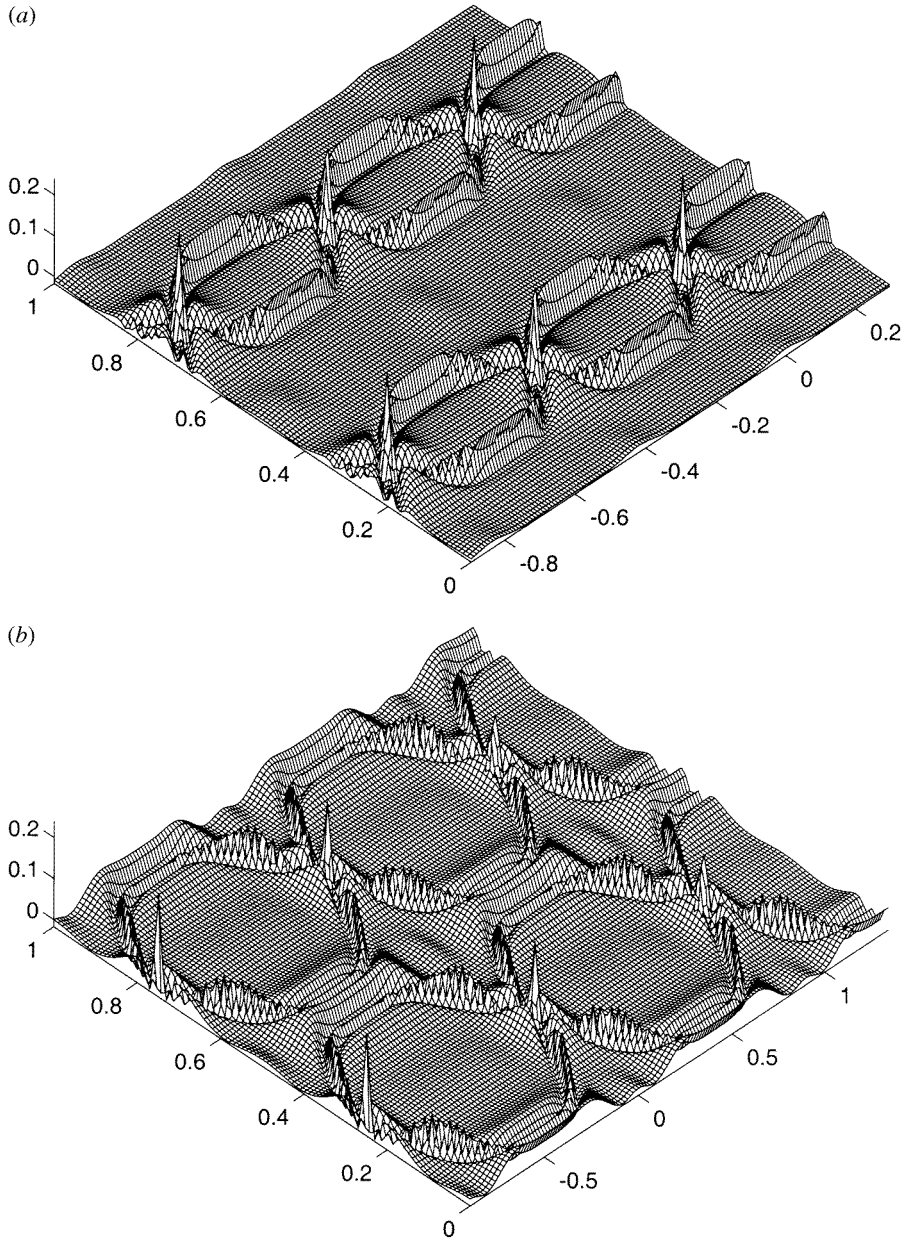

Figure 12. Chain (*a*), hexagonal (*b*) and square (*c*) patterns generated by analytic solution (98) in the x–t plane.

$$\times(1 - 4h^2 i^2 \pi^2 L^{-2}/3)].$$

We assumed that $H_i = 0$ and amplitude A_i is very small or imaginary. Then constants $C_{i\pm}$ are real if $h^2 \geqslant 0.75 i^{-2}\pi^{-2}L^2$. In this case, counterintuitive standing arch-like waves are generated:

$$u_\pm = \pm \sum_i (2h^2/9 - 8i^{-2}\pi^{-2}L^2/3)^{0.5} \sin 2\pi i x L^{-1}. \tag{109}$$

(*c*)

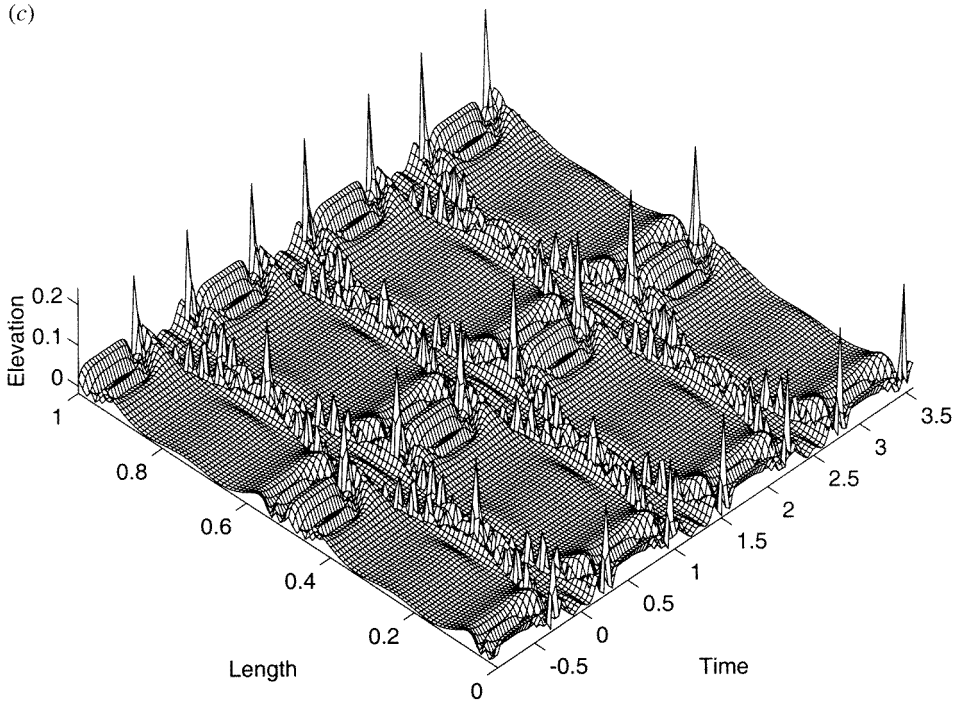

Figure 12. (Continued)

The 'arching' phenomenon was observed clearly [37, 38] when the acceleration was higher than $8g_0$. The layer could form a few static arches during the flight. The form changes due to the layer–bottom collision. In particular, two different states of the layer are clearly visible in figure 3 from [37].

It follows from (109) that the thicker (thinner) the layer, the lower (higher) the harmonics are excited. Let us assume that the different signs in (109) correspond to the different states of the layer. As a result, we can construct the next subharmonic periodical solution of equation (80):

$$u = [H(\sin m_*^{-1}\omega t) - H(-\sin m_*^{-1}\omega t)] \sum_i (2h^2/9 - 8i^{-2}\pi^{-2}L^2/3)^{0.5} \sin 2\pi i x L^{-1}. \quad (110)$$

Here H is the Heaviside function and $m_* = 2, 4, 6, \ldots$. The waves obtain the opposite phase instantly during the layer–bottom collision. One can see that solution (110) qualitatively describes observations [37, 38].

It follows from this consideration that both topographic and parametric effects may be important for the deep beds. The former can define harmonics which generate at the beginning of the excitation even if the layer is initially practically flat (topography is very small). In particular, topographic resonance ($\omega^2 = (\pi i a_0/L)^2$) can take place (see (23)). The development of these harmonics, when the excitation is increased, depends on the parametric effect.

When the excitation is intensified then small-amplitude waves transform into arch waves. The period of oscillations of these last waves depends on the flying time. At the beginning, the arch waves oscillate at precisely half the forcing frequency ($m_*^{-1} = 2$ in (110)). Then, a series of the doubling bifurcations can occur ($m_*^{-1} = 4, 6, \ldots$) and the system can move to chaos [37, 38].

4.5. Parametric–topographic resonant waves

If the amplitude of the standing or arch parametric waves is large enough then a periodical horizontal force generates during the collisions. As a result, horizontally forced standing waves may be generated in addition to the parametric waves. Of course, the former are smaller than the latter if the forced frequency is not close to the natural horizontal frequencies Ω_{lN} of the layer or $\omega^2 \neq (\pi i a_0/L)^2$ (see (23)). However, at the resonances the forced waves may be larger than the parametric waves. Thus, we suggest that counterintuitive travelling waves generate on the free surface at the above resonances.

Indeed, these travelling waves were observed in the Faraday experiments with initially flat granular layers (see [8, 39] and figure 15 from [38]). One can easily calculate that the waves in figure 14 of [38] correspond to the second horizontal resonance while the waves in [39] correspond to the second ($L = 150$ mm) or fourth horizontal resonances ($L = 300$ mm). The theory presented in section 2 is completely applicable for these parametric–topographic excited waves. Therefore, this case is not additionally considered. However, we note that figure 1 apparently describes the solitary burst presented in figure 5 from [39].

5. Discussions and conclusion

Topographic effect in the Faraday experiments. We have considered different topographies as natural resonators. In particular, a layer of a variable thickness was considered as the topography. The perturbed wave equation (13) was derived in which a forced term was generated because of the topography. Both d'Alembert-type (21) and non-d'Alembert-type (94) solutions and waves were presented. It was found that in different finite dissipative–dispersive physical systems nonlinear waves may exist which are impossible to classify as well known soliton-, cnoidal-, shock- or breather-type waves. However, these waves are described approximately by the same expressions: (51), (53), (55), (79) and (98). In particular, solution (98) describes *spatiotemporally oscillating*, localized, nonlinear, surface waves which can have properties of both *standing* waves and *travelling* waves (see figures 10 and 11). Different wave patterns were yielded by the solutions (see figures 1–3, 5, 10–12 and [40]). It was found that, on the one hand, anomalous forced, free and parametric waves may be generated in the topography. On the other hand, topographic, nonlinear and resonant effects explain some anomalous results of both experiments and earthquakes. The quadratic nonlinear free and parametric waves may be generated in layers only due to the topographic effect or/and an initial deformed state. More intensive waves, for which the cubic term in the perturbed wave equation is important, may be excited in the flat layers.

The shallow arch waves were described. We must note that sometimes strictly localized travelling waves generate on the water surface additionally to the smooth standing waves. As a result complex wave patterns are formed. These patterns have been studied in [24, 36].

It follows from the theory that the velocity of the surface waves in the Faraday experiment is defined by the vertical excitation, geometrical and mechanical properties of a layer. According to (13) the velocity of these waves depends on the thickness of the layer and the dispersion. On the other hand, the wave velocity is defined by the elastic shear modulus. Because of the vertical acceleration the wave can stop and change direction of motion (see figures 10–12 and [24]) (this anomalous behaviour is reminiscent of the behaviour of planets in the Ptolemy model of the Universe). The effect of the voidage may be very important for the wave velocity. Thus this velocity may be quite different from well known velocities of the shear, Rayleigh or Love waves. In particular, for gassy or liquefied soils the shear velocity is of the order of 10 m s^{-1} and we can have $a_s \leqslant a_f$ in (13). Some clays can have a high water content. For

example, Mexico City clay has $a_s \approx 80$ m s^{-1} [11]. During the September 19, 1985 Michoacan earthquake the greatest damage occurred there where a soil thickness changes from 38 to 50 m, where $a_f \approx 20$ m s^{-1}. One can see that an effect of a_f may be important for a prediction of behaviour of the natural resonators during earthquakes.

The Faraday experiments realized by Nature. Hills, sedimentary basins, lakes, and a continental shelf are natural resonators. According to the theory, under the vertical earthquake-induced excitation these topographies can demonstrate strictly nonlinear behaviour. In particular, in these topographies waves may be generated which recall the waves observed in the Faraday experiments. Forced, free or parametric waves may be generated by an earthquake in the natural resonators.

Subharmonic, localized, nonlinear, free waves may be excited in the elongate topographies during earthquakes due to a sole shake. Indeed, sometimes a sole seismic shake may be trapped by the topography. The frequency of the reverberations of the trapped waves can slowly reduce or increase, for example, because of the slope of boundaries. As a result, the above-discussed trans-resonant evolution of waves (see figures 4, 6, 8 and 9) can occur. If the frequency of trapped waves increases because of the reverberation, then their amplitude reduces after the resonance (see figures 6 and 8). If the frequency of trapped waves reduces, then their amplitude can increase after the resonance (see figures 6 and 9). Therefore, a collapse of structures on the surface of the topography can occur when the initial seismic waves had passed if the frequency of the reverberations of the trapped waves inside of the topography reduces.

Charles Darwin noted, in similar fashion, some results of the 20 February 1835 Chilean earthquake for a small island of Quiriquina:

> '... The ground was fissured in many parts, in north and south line; which direction perhaps was caused by the yielding of the parallel and steep sides of the narrow island. Some of the fissures near the cliffs were a yard wide...' [10].

Very long seismic waves excited the shelf and, perhaps, vertically vibrated the base of the island. Because of the slope of the shelf, the horizontal component of the disturbing vertical force was generated and the resonant waves were excited in the topography. Water surrounds the island; therefore, the cliffs may be considered as approximately fixed and the theory of section 2 is applicable. Therefore, shock-like waves (see figures 1(*a*) and 1(*d*)) might have been generated on the surface of Quiriquina. The material near the cliffs yields to the tension more than the material inside of the island, therefore the fissures near the cliffs of Quiriquina were wider.

According to the theory, the trans-resonant seismic waves in a topography can have the order $l^{1/2}$ (see, for example, (28)) or $l_*^{1/3}$ (see, for example, (68)). As a result, if the dimensionless amplitude of the bed oscillations is 0.001, then the nonlinear theory predicts the wave amplitude to be of the order of $(0.001)^{1/2}$ or 0.1, respectively. This dramatic result qualitatively agrees with results of some observations [11, 26–28]. Thus, earthquake damage of structures located on the surface or near the natural topography (resonator) may be much more dependent upon the resonator properties than on the proximity or intensity of earthquake sources.

Thus, the solutions presented in this paper describe *unfamiliar* nonlinear seismic waves. Most seismologists, apparently, have tended to dismiss nonlinear effects as a second-order nuisance, although nonlinear aspects of the propagation and the amplification of seismic waves have begun to be discussed intensively (see *Bull. Seismol. Soc. Am.* **88**, no 6, 1998). We have found that nonlinear effects in natural resonators may be very important.

Conclusion. The objective of this paper was a better understanding of the influence of topographies on the nonlinear wave processes in bounded dispersive and dissipative media. On the other hand, we obtained solutions unknown in nonlinear dynamics. Perhaps, these solutions describe waves in different wave fields of Nature. Indeed, these solutions describe the water waves which were simulated earlier with the help of the numerical solution of the Schrödinger equation [34]. At the same time these analytical solutions describe qualitatively some results of the numerical solutions of the Swift–Hogenberg equation (see figures 12.2–12.4 from [41]). It was found that the Maxwell-type wave equation and the so-called scalar ϕ^4 field equation can have the same solutions [40]. In particular, expression (79) defines the wave-particle solution for the field if $c = 0$. Waves, which are reminiscent of the waves presented here, may be generated in spherical symmetrical systems according to [42–44]. Thus, we showed that the above solutions and the methods of nonlinear acoustics [45] allow one to study various wave fields in Nature.

References

[1] Faraday F 1831 *Phil. Trans. R. Soc.* A **121** 299–340
[2] Rayleigh Lord 1883 *Phil. Mag.* **15** 229–35
Rayleigh Lord 1883 *Phil. Mag.* **16** 50–8
[3] Benjamin T B and Ursell F 1954 *Proc. R. Soc.* A **225** 505–15
[4] Miles J and Henderson D 1990 *Ann. Rev. Fluid Mech.* **22** 143–65
[5] Jaeger H J, Nagel S R and Behringer R P 1996 *Rev. Mod. Phys.* **68** 1259–73
[6] Umbanhowar P B, Melo F and Swinney H L 1996 *Nature* **382** 793–6
[7] Mukerjee M 1996 *Sci. Am.* **275** 28–36
[8] Cerda E, Melo F and Rica S 1997 *Phys. Rev. Lett.* **79** 4570–3
[9] Shinbrot T 1997 *Nature* **389** 574–6
Tsimring L S and Aranson I S 1997 *Phys. Rev. Lett.* **79** 213–6
Venkataramani S C and Ott E 1998 *Phys. Rev. Lett.* **80** 3495–8
[10] Darwin C 1986 *Journal of Researches (The works of Charles Darwin)* vol 3, ed P H Barrett and R B Freeman (Cambridge: Cambridge University Press) p 290
[11] Singh S K, Mena E and Castro R 1988 *Bull. Seismol. Soc. Am.* **78** 451–77
[12] Galiev Sh U 1997 *Proc. 5th Int. Congress on Sound and Vibration (Adelaide, December)* (Adelaide: University of Adelaide) pp 1785–96
[13] Galiev Sh U and Galiev T Sh 1998 *Phys. Lett.* A **246** 299–305
[14] Lamb H 1932 *Hydrodynamics* 6th edn (New York: Dover) p 259
[15] Chester W 1968 *Proc. R. Soc.* A **306** 5–22
[16] Boussinesq J 1872 *J. Math. Pure Appl.* **17** 55–108
[17] Rudenko O V and Soluyan S L 1977 *Theoretical Foundations of Nonlinear Acoustic* (Plenum: Consultants Bureau)
[18] Galiev Sh U and Panova O P 1995 *Strength Mat.* **27** 602–20
Galiev Sh U 1997 *Int. J. Impact Engng* **19** 345–59
[19] Harris S E and Crighton D G 1994 *J. Fluid Mech.* **266** 243–76
[20] Abdullaev F Kh 1989 *Phys. Rep.* **179** 1–78
[21] Galiev Sh U 1972 *Mech. Tverdogo Tela* **4** 80–7
[22] Chester W and Bones J B 1968 *Proc. R. Soc.* A **306** 23–39
[23] Kuznetsov V V, Makoryakov V E, Pokusaev B G and Shreiber I R 1978 *J. Fluid Mech.* **85** 85–96
[24] Galiev Sh U 1998 Is there some new kind of nonlinear surface waves? *The University of Auckland, School of Engineering Report No. 584*
[25] Sibgatullin N R 1972 *J. Appl. Math. Mech.* **36** 70–8
[26] Spudich P, Hellweg M and Lee W H K 1996 *Bull. Seismol. Soc. Am.* **86** S193–208
[27] Rail J A 1996 *Bull. Seismol. Soc. Am.* **86** 1714–23
[28] Shakal A F, Huang M J and Darragh R B 1996 *Bull. Seismol. Soc. Am.* **86** S231–46
[29] Zeng X and Schofield A N 1996 *Geotechnique* **46** 83–102
[30] Natanzon M S 1977 *Longitudinal Self-Excited Oscillations of a Liquid-Fuel Rocket* (Moscow: Mashinostroenie) (in Russian)

[31] Galiev Sh U, Yakovtsov A V and Zelenyuk N I 1987 *Strength Mat.* **19** 1715–20
Galiev Sh U 1988 *Nonlinear Waves in Bounded Continua* (Kiev: Naukova Dumka) (in Russian)
[32] Mujica N and Melo F 1998 *Phys. Rev. Lett.* **80** 5121–4
[33] Melo F, Umbanhowar P and Swinney H L 1995 *Phys. Rev. Lett.* **75** 3838–41
[34] Wang X and Wei R 1997 *Phys. Rev. Lett.* **78** 2744–7
[35] Bizon C, Shattuck M D, Swift J B, McCormick W D and Swinney H L 1998 *Phys. Rev. Lett.* **80** 57–60
[36] Galiev Sh U 1999 *Phys. Lett.* A submitted
[37] Douady S, Fauve S and Laroche C 1989 *Europhys. Lett.* **8** 621–7
[38] Wassgren C R, Brennen C E and Hunt M L 1996 *ASME J. Appl. Mech.* **63** 712–9
[39] Clement E, Vanel L, Rajchenbach J and Duran L 1996 *Phys. Rev.* E **53** 2972–5
[40] Galiev Sh U 1999 *UpoN'99: Proc. 2nd Intern. Conf. on Unsolved Problems of Noise and Fluctuations (Adelaide, July 1999)* (Adelaide: University of Adelaide) pp 321–6
[41] Mandel P 1997 *Theoretical Problems in Cavity Nonlinear Optics* (Cambridge: Cambridge University Press)
[42] Galiev Sh U 1998 *Proc. Int. Congress on Noise Control Engineering (Christchurch, November 1988)* (New Zealand Acoustical Society) pp 287–92
[43] Galiev Sh U 1998 *Proc. 13th Conf. on Australasian Fluid Mechanics (Melbourne, December)* (Monash University) pp 1027–30
[44] Galiev Sh U 1999 *Phys. Lett.* A accepted for publication
[45] Crighton D G 1979 *Ann. Rev. Fluid Mech.* **11** 11–33